

---


Electronic Theses and Dissertations, 2004-2019

---

2006

## Demonstrating Reflectarray Behavior At Infrared

James Ginn  
*University of Central Florida*

 Part of the [Electrical and Electronics Commons](#)  
Find similar works at: <https://stars.library.ucf.edu/etd>  
University of Central Florida Libraries <http://library.ucf.edu>

This Masters Thesis (Open Access) is brought to you for free and open access by STARS. It has been accepted for inclusion in Electronic Theses and Dissertations, 2004-2019 by an authorized administrator of STARS. For more information, please contact [STARS@ucf.edu](mailto:STARS@ucf.edu).

---

### STARS Citation

Ginn, James, "Demonstrating Reflectarray Behavior At Infrared" (2006). *Electronic Theses and Dissertations, 2004-2019*. 836.  
<https://stars.library.ucf.edu/etd/836>

DEMONSTRATING REFLECTARRAY BEHAVIOR AT INFRARED

by

JAMES C. GINN, III  
B.S. University of Central Florida, 2004

A Thesis submitted in partial fulfillment of the requirements  
for the degree of Master of Science  
in the School of Electrical Engineering and Computer Science  
in the College of Engineering and Computer Science  
at the University of Central Florida  
Orlando, Florida

Spring Term  
2006

© 2006 James Ginn

## ABSTRACT

Reflectarrays are traditionally passive, planar microstrip antenna devices designed for reflected phase manipulation at each individual antenna element making up the array. By varying the phase response across the surface with the antenna elements, reflectarrays allows a planar surface to exhibit electromagnetically an arbitrary geometry, such as a spherical surface. Initially proposed as a low-cost replacement for bulky parabolic reflectors, reflectarrays have been successfully developed and utilized at both RF and millimeter-wave frequencies. From the standpoint of an optical systems designer, adapting low-frequency reflectarray technology to develop a sub-millimeter and infrared reflectarray (SMIR) would provide a highly desirable alternative to similarly behaved polished or diffractive optical devices. Compared to traditional optical reflectors, SMIRs should be cheaper to fabricate, have a smaller physical footprint, allow for utility stacking, and encourage direct integration of aberration correction.

To demonstrate the feasibility of utilizing reflectarray technology at infrared (IR), a simple SMIR proof of concept has been successfully designed, fabricated, and tested. The SMIR is comprised of three independent arrays or “stripes” of a single size element on a coated optical flat. Actual reflectarray elements consist of variable size patches that exhibit higher operating bandwidths than reflectarrays utilizing other types of elements and are easier to fabricate at small dimensions. For testing, each stripe element has been chosen to exhibit a unique phase shift for measurement using an IR interferometer.

Preliminary investigation of future reflectarray development is also discussed. Emphasis is placed on improving operating bandwidth, development of a planar focusing element, and

aberration correction. With further development, SMIR technology should present a powerful tool for low cost, flexible optical system design.

To Grandma, I miss you.

## ACKNOWLEDGMENTS

Dr. Brian Lail, my thesis chair, for his constant patience, guidance, and support beginning when I was a mere undergraduate freshman at the University of Central Florida learning the principles of Electrical Engineering.

Dr. Glenn Boreman for whom I am grateful for the opportunity to participate in the IR Systems Lab and who has always encouraged and aided in my research.

Dr. Arthur Weeks for agreeing to again serve on my thesis committee and for his feedback regarding my research.

Lockheed Martin Missile and Fire Control for their continued financial and logistical support of my infrared reflectarray research. I would like to specifically acknowledge Edit Braunstein, Gene Tener, and Thomas Haberfelde. I would especially like to acknowledge Darren Zinn for his help in device measurement with the IR interferometer.

The other members of the FSS team, Jeff Tharp and Dave Shelton, for providing an invaluable source of support and input through out the entire thesis process.

Charles Middleton for his patience and direction during the reflectarray fabrication process.

Guy Zummo for seemingly always finding solutions to my problems in the clean room.

All of the members of the IR Systems lab that I am honored to have worked with and look forward to the opportunity to continue to work with: Todd Du Bosq, Peter Krenz, Tasneem Mandviwala, Chris Middlebrook, Sid Pandey, Dan Mullally, Dr. Ray Folks, Dr. Jose Lopez-Alonso, Dr. Ivan Divliansky, and Dr. Brian Monacelli.

My friends and family for always being there for me and providing me with a constant source of personal inspiration.

Mom and Dad, I can never thank you enough.



# TABLE OF CONTENTS

LIST OF TABLES .....	ix
LIST OF FIGURES .....	x
LIST OF SYMBOLS/ABBREVIATIONS .....	xi
CHAPTER 1: INTRODUCTION .....	1
1.1 Beamforming Antennas .....	1
1.1.1 Notable Example: Reflector Antennas .....	1
1.1.2 Notable Example: Phased Array Antennas .....	5
1.1.3 Summary of Phased Arrays and Reflector Antennas .....	8
1.2 Reflectarray Antenna .....	9
1.3 Statement of Thesis .....	11
1.4 Infrared Reflectarray Development Motivation .....	12
CHAPTER 2: FUNDAMENTALS OF REFLECTARRAY DESIGN .....	14
2.1 The Variable-Patch Reflectarray .....	14
2.2 Circuit Equivalent Design: The Transmission Line Approach .....	15
2.3 Characterization Through Numerical Modeling .....	19
2.3.1 Finite Element – Single Element Modeling .....	21
2.3.2 Finite Element – Infinite Element Modeling .....	23
2.3.3 Periodic MoM Modeling .....	24
CHAPTER 3: DEVICE SIMULATION AND MODELING .....	26
3.1 Initial Device Specification .....	26
3.2 Reflectarray Simulation Results .....	27
CHAPTER 4: DEVICE FABRICATION .....	29
4.1 Device Layout .....	29
4.2 Fabrication Methodology .....	30
4.3 Fabricated Devices .....	36
CHAPTER 5: DEVICE TESTING AND RESULTS .....	42
5.1 Testing Methodology .....	42
5.2 Measured Results .....	45
5.3 Result Analysis .....	46
CHAPTER 6: CONCLUSIONS .....	53
6.1 Summary of Results .....	53
6.2 Future Work .....	55
6.2.1 Planar Tilt and Focusing Elements .....	55
6.2.2 EBGs and Antenna Miniaturization .....	56
6.2.3 Bandwidth Improvement .....	57
6.2.4 Aberration Correction .....	60
6.2.5 Further Cost Reduction .....	61
LIST OF REFERENCES .....	63

## LIST OF TABLES

Table 1.1: Comparison of Parabolic Reflector and Phased Array Antennas.....	9
Table 3.1: Initial Model Specifications.....	27
Table 5.1: Measured Relative Phase Shift vs. Reflectarray Patch Size.....	52
Table 6.1: Further Reflectarray Cost Reduction Techniques.....	62

## LIST OF FIGURES

Figure 1.1: Parabolic Reflector with Planar Wavefront.....	3
Figure 1.2: Phased Array with Spherical Wavefront.....	6
Figure 1.3: Planar Reflectarray Exhibiting a Parabolic Geometry.....	10
Figure 2.1: Variable-Patch Reflectarray Layout.....	14
Figure 2.2: Reflectarray Transmission Line Equivalent.....	16
Figure 2.3: Smith Chart plot of $\Gamma_{in}$ Demonstrating Reflectarray Phase Transition by Varying Patch Size.....	18
Figure 2.4: Model Layout for FEM Single Element Reflectarray Modeling.....	22
Figure 2.5: Model Layout for FEM Infinite Array Reflectarray Modeling.....	24
Figure 2.6: Model Layout for Periodic MoM Reflectarray Modeling.....	25
Figure 3.1: Measured Dielectric Properties for $ZrO_2$ .....	26
Figure 3.2: Comparison of Modeled Results.....	28
Figure 4.1: Proof of Concept SMIR Layout.....	29
Figure 4.2: Optical Flat Coating Process.....	31
Figure 4.3: Bi-layer Resist.....	33
Figure 4.4: SMIR E-Beam Holder.....	34
Figure 4.5: E-Beam Development Process.....	35
Figure 4.6: Evaporation and Lift-off.....	36
Figure 4.7: SEM image of Metalized Dose Matrix.....	37
Figure 4.8: Visible Image of Metalized Dose Matrix.....	38
Figure 4.9: Comparison of Modeled and Predicted Phase.....	39
Figure 4.10: Fabricated Strip SMIR with Reference Sizes.....	40
Figure 4.11: SEM Image of One of the Stripes of the Fabricated SMIR.....	40
Figure 4.12: Visible Image of One of the Stripes of the Fabricated SMIR.....	41
Figure 5.1: Twyman-Green Interferometer [3.1].....	43
Figure 5.2: Interferogram of Coated Wafer.....	46
Figure 5.3: Interferograms of Fabricated SMIRs.....	46
Figure 5.4: Averaged Phase Response Results for First SMIR.....	48
Figure 5.5: Smoothed Phase Response Results for First SMIR.....	49
Figure 5.6: Averaged Phase Response Results for Second SMIR.....	50
Figure 5.7: Smoothed Phase Response Results for Second SMIR.....	51
Figure 6.1: Comparison of Measured and Modeled Results.....	54
Figure 6.2: Example Multi-band Reflectarray Layout.....	58
Figure 6.3: Measured Permittivity of $ZrO_2$ Exhibiting Linear Transition.....	59
Figure 6.4: Stackup for a Multi-Layer Reflectarray.....	60

## LIST OF SYMBOLS/ABBREVIATIONS

AF.....	Array Factor
dB.....	Logarithmic Power Ratio
deg.....	Degree
$\epsilon_r$ .....	Dielectric Constant
e-beam.....	Electron Beam
EBG.....	Electromagnetic Bandgap
FEM.....	Finite Element Method
FSS.....	Frequency Selective Surface
IR.....	Infrared
IPA.....	Isopropyl Alcohol
LWIR.....	Long-Wave Infrared
m.....	Meter
mm.....	Millimeter ( $10^{-3}$ Meter)
MoM.....	Method of Moments
MPIE.....	Mixed-Potential Integral Equation
MWIR.....	Mid-Wave Infrared
$\mu\text{m}$ .....	Micrometer ( $10^{-6}$ Meter)
nm.....	Nanometer ( $10^{-9}$ Meter)
PEC.....	Perfect Electric Conductor
PMC.....	Perfect Magnetic Conductor
RF.....	Radio Frequency
SMIR.....	Sub-Millimeter and Infrared Reflectarray
SEM.....	Scanning Electron Microscope
THz.....	Terahertz ( $10^{12}$ Hertz)
$\tan\delta$ .....	Loss Tangent
UAV.....	Unmanned Aerial Vehicle
ZrO <sub>2</sub> .....	Zirconium Dioxide

# CHAPTER 1: INTRODUCTION

## 1.1 Beamforming Antennas

Beamforming antennas are a sub-class of antennas comprising of an array of antenna elements characterized by their ability to collectively exhibit a narrow radiated beamwidth or a focusing wavefront [1.1]. Beamforming antennas are highly directive antennas that find heavy usage at microwave frequencies where omni-directional antennas would be undesirable, such as in satellite communication systems, line of sight transmission systems, and scannable detectors. At higher frequencies, including visible and infrared (IR) frequencies, beamforming antennas are often deployed as focusing elements, directional detectors, and collimators. Although highly valued, beamsteering antennas are not without their limitations. Two popular beamforming antenna configurations, the reflector antenna and the phased array, will be briefly considered to demonstrate the weakness and advantages of conventional beamforming antennas.

### **1.1.1 Notable Example: Reflector Antennas**

Reflector antennas are one of the oldest and simplest known antenna devices and have been deployed, in various forms, across the entire electromagnetic spectrum. In its most basic configuration, the reflector antenna is simply a reflective surface of arbitrary geometry impinged upon by electromagnetic radiation. Thus, the planar mirror could be viewed as the earliest developed reflector antenna. From the planar mirror, additional reflector antenna geometries have been developed at visible frequencies, such as the focusing, spherical mirror. Reflector antenna development at microwave frequencies did

not began to mature until World War II to meet the needs of the emerging field of radar [1.2]. Now sold commercially for use in receiving telecommunication and television signals, radio frequency (RF) reflector antennas continue to increase in popularity as an integral part of most satellite communication systems [1.3].

Although several reflector antenna geometries have been used in the past, one of the most popular geometries is the center-fed parabolic reflector. In the ideal center-fed parabolic antenna reflector configuration, a point source is placed at the center of focus of the paraboloidal reflector. Fields radiated from an ideal point source will inherently have a spherical wavefront and when the radiated spherical wavefront impinges on the paraboloidal shaped reflective surface, a planar or collimated wavefront will reflect. Changing the wavefront of the feeding source or the physical geometry of the reflector antenna will change the reflected wavefront, for example, if the source in the previous example is replaced with a plane wave source, the reflected wavefront will become spherical or if the reflector antenna is planar, the reflected wavefront will remain spherical. Therefore, by knowing the incident feed wavefront it is possible to reflect an arbitrary wavefront back through control of the physical geometry of the reflector antenna.

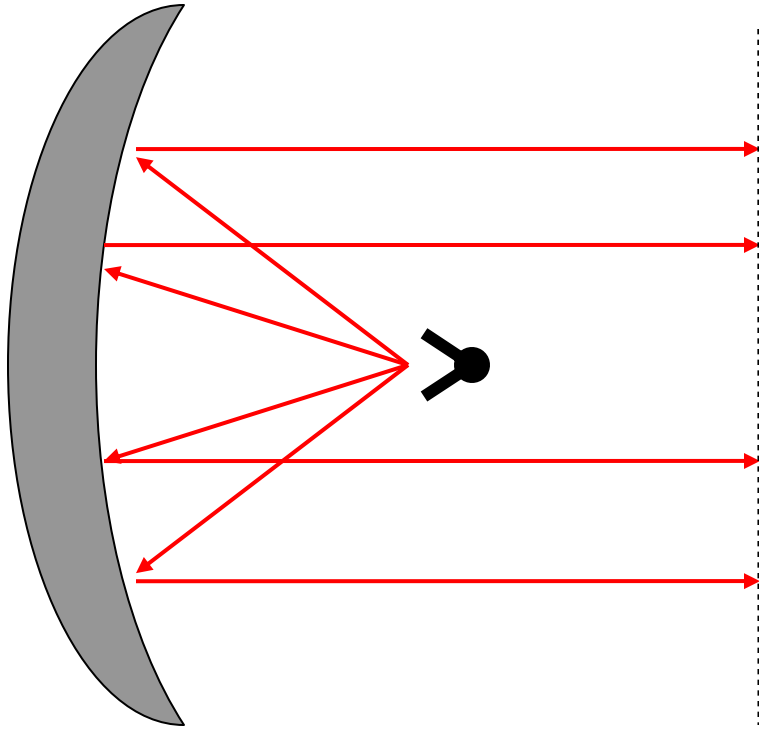


Figure 1.1: Parabolic Reflector with Planar Wavefront

Analysis of the parabolic reflector antenna and most conventional reflector antennas can be carried out using an optical technique known as ray tracing [1.4 – 1.6]. Ray tracing is a technique for following wavefront propagation through an optical system by applying Snell’s law at each surface of the optical system to rays that flow perpendicular to the propagating wavefront. For the reflector antenna, only Snell’s law of reflection is needed [1.7], or

$$\hat{r}_{reflected} = \hat{r}_{incident} - 2\hat{n}(\hat{r}_{incident} \cdot \hat{n}) \quad \text{Eq. 1-1}$$

where the normal is the normal of the reflector surface at the point of incidence. Clearly, the direction of the unit vector of the normal of the reflector surface that the incident ray

observes is only dependent on the physical sag, or shape, of the reflector surface and the position of the source to the point of incidence. Thus, by knowing the impinging wavefront from the source and the position of the source, it is possible to choose reflector geometries to introduce arbitrary wavefronts upon reflection simply by sampling across the plane in which the reflector will be placed. Numerous commercially available ray tracing design packages utilize this exact approach and support reflector development and characterization natively [1.8 – 1.9].

The main advantage for reflector antennas, aside from simplistic design procedure, is their potential for high radiation efficiency. Across the electromagnetic spectrum, known high conductivity materials allow for low-loss upon reflection by the reflector antenna. Without active components, reflector antennas are well suited for high power applications and rarely need maintenance. In addition, with the capability of collimation, reflector antennas exhibit high gain – often exceeding 60 dB at RF frequencies [1.3].

Even with its numerous advantages, the reflector antenna exhibits several distinctive limitations. In the traditional spherical and parabolic configurations, the reflector is inherently bulky. Unlike planar antennas, the parabolic reflector, traditionally physically thicker to maintain proper shape, prohibits folding for transport. Resulting from the fact wavefront modification occurs due to physical path length differences, reflector antennas cannot be made conformal, which restricts deployment on mobile structures, such as vehicles or aircraft, where drag may become a concern. At shorter wavelengths, the cost of fabrication increases because of increased sensitivity to height variations on the antenna surface and diffraction at the edge of the reflector becomes a



concern. Additionally, utility stacking of reflector antennas and other devices, such as frequency selective surfaces (FSS), is difficult or completely impossible.

### **1.1.2 Notable Example: Phased Array Antennas**

Phased arrays share several similarities with reflector antennas in terms of their ability to control radiated wavefronts and exhibit high directivity. Phased arrays are traditionally active, planar devices, which, by introducing a progressive feed phase delay between neighboring elements, will radiate only in a specified direction or with a specific wavefront [1.10]. The simplest developed phased array consists of a large array of aperture antennas fed by a single source, but with each antenna connected to the source by a different length of waveguide. The waveguide length difference between the aperture antennas introduces a phase delay in the radiated fields of each horn, which, in turn, changes the array's far-field pattern to add constructively in only a specific direction or exhibit an arbitrary wavefront. Planar, microstrip phased arrays behave in the exact same way, with progressive phase difference introduced by waveguide length or lumped elements.

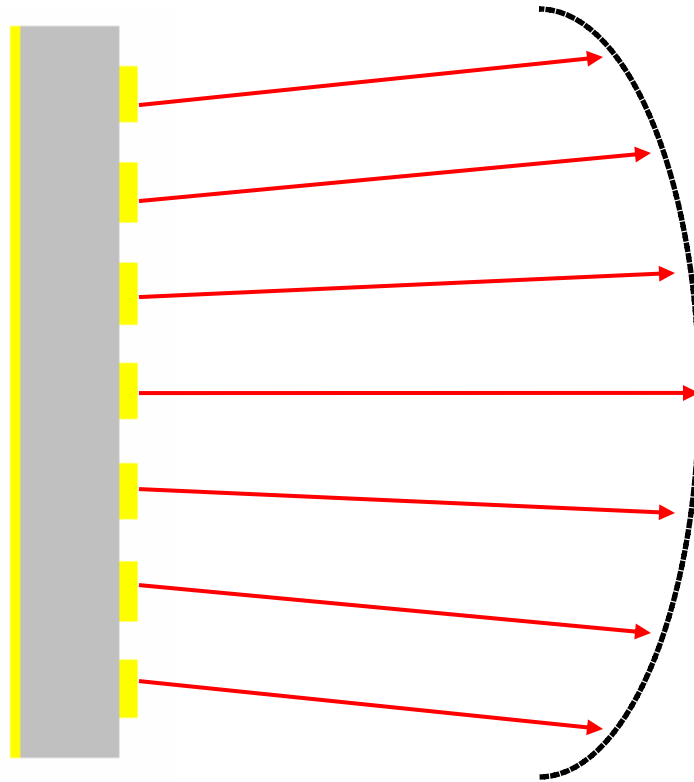


Figure 1.2: Phased Array with Spherical Wavefront

Beamforming by the phased array can be explored using the analysis outlined by Balanis [1.11] and considering the simplified phased array of an  $N \times N$  layout of identical, equally spaced radiating antenna elements. If we know the radiated electric field of a single element by itself, and neglecting inter-element coupling, we can calculate the radiated electric field of the array by:

$$E_{array} = E_{element} \times AF \quad \text{Eq. 1-2}$$

where  $AF$  is the array factor of the phased array. The normalized array factor of an  $N \times N$  uniform array can be written expressed as:

$$AF_n = \left[ \frac{1}{N} \frac{\sin(\frac{N}{2}\Psi_x)}{\sin(\frac{\Psi_x}{2})} \right] \left[ \frac{1}{N} \frac{\sin(\frac{N}{2}\Psi_y)}{\sin(\frac{\Psi_y}{2})} \right] \quad \text{Eq. 1-3}$$

$$\Psi_x = kd \sin \theta \cos \phi + \beta_x$$

$$\Psi_y = kd \sin \theta \sin \phi + \beta_y$$

where  $d$  is the array spacing distance between each element,  $k$  is the wave number, and  $\beta$  is the progressive phase difference between each element. If the feed amplitude remains the same for each element, the progressive phase difference between each element ( $\beta_x$ ,  $\beta_y$ ) will determine the direction of the main beam ( $\theta_0$ ,  $\phi_0$ ), or:

$$\begin{aligned} \beta_x &= -kd \sin \theta_0 \cos \phi_0 \\ \beta_y &= -kd \sin \theta_0 \sin \phi_0 \end{aligned} \quad \text{Eq. 1-4}$$

From the equations 1-3 and 1-4, it is clear that antenna's directivity is a product of the array spacing and the directivity of the element making up the array. Thus, phased arrays can be designed to achieve high directivities comparable to the directivity of a reflector antenna. Additionally, the utilization of a non-uniform array arrangement allows for further control of the radiated far-field pattern and is essential to introduce non-planar wavefronts.

The significant difference between the reflector antenna and the phased array is that the phased array is not dependent on a physical height difference to alter the radiated wavefront. This allows the phased array to be significantly thinner than the reflector antenna and allows the antenna to be designed for conformal deployment with correction for height differences occurring in the progressive phase delay [1.12]. Phased arrays can

also be tuned by introducing a phase delay at the source and, through lithography, can be designed to exhibit far more complicated radiated wavefronts.

Unlike reflector antennas, phased arrays exhibit many of the limitations common to most planar antennas. Often inefficient with low power excitation, phased arrays cannot handle high power sources without physical breakdown [1.11]. Additionally, phased arrays are inherently active devices and, thus, cannot be utilized as an intermediate focusing element. Analysis of phased arrays, especially when accounting for coupling or when using non-uniform arrays, is far more complicated than reflector antennas and will often demand the use of a numerical analysis.

### **1.1.3 Summary of Phased Arrays and Reflector Antennas**

Table 1.1 presents a brief summary of the advantages and disadvantages of using a parabolic reflector or a phased array antenna as a beamforming antenna. From the table, it is clear that both antennas exhibit significant limitations that will restrict design and deployment flexibility. However, the two antennas utilize similar electromagnetic phenomena for beamsteering and wavefront modification, therefore, a hybrid reflector - phased array antenna exhibiting the advantages of both antennas should be feasible. Thus, the desire for such a device led to the development of a new type of antenna known as the reflectarray.

**Table 1.1: Comparison of Parabolic Reflector and Phased Array Antennas**

	<b>Parabolic Reflector</b>	<b>Phased Array</b>
<b>Directivity</b>	High	High
<b>Efficiency</b>	High	Low
<b>Design Complexity</b>	Fairly Simple	Complex
<b>Passive</b>	Yes	No
<b>Intermediate Element</b>	Yes	No
<b>Conformal</b>	No	Yes
<b>Easily Folded</b>	No	Yes

### **1.2 Reflectarray Antenna**

The reflectarray antenna, in its most simple form, is passive, planar microstrip antenna array designed for reflected beamforming. By varying the scattered phase response across the surface through the array elements, reflectarrays allow a planar surface to exhibit electromagnetically an arbitrary geometry upon reflection (Figure 1.3). Like the phased array, the far-field pattern of the reflectarray can be found by summing the scattered far-field pattern radiated by each of the individual elements in the array and, similarly, the reflectarray has a very small physical footprint, can be conformal, allows fabrication using traditional lithography techniques, and grants the possibility of utility stacking [1.13]. As a passive device, the reflectarray inherits many of the advantageous characteristics of the reflector antenna including simplified design using ray tracing and relatively low loss. The combination of these beneficial capabilities makes reflectarrays highly desirable for use in a multitude of antenna systems [1.14].

From a conceptual standpoint, the individual microstrip elements making up the reflectarray can be viewed as direct reflector/phased array hybrid. When radiation impinges on an element in the reflectarray the phase delay introduced upon reflection

relative to the neighboring elements will be entirely a product of the spacing difference between each element (path difference) and physical dimension differences between the elements (feed phase difference). Most reflectarray designs have fixed element periodicity for simplicity, and instead simply varied the dimensions of the array element to change the surface impedance at the point of the element to introduce the desired phase shift in the same way that the phased array will vary waveguide lengths or the reflector will vary curvature to create the desired phase delay.

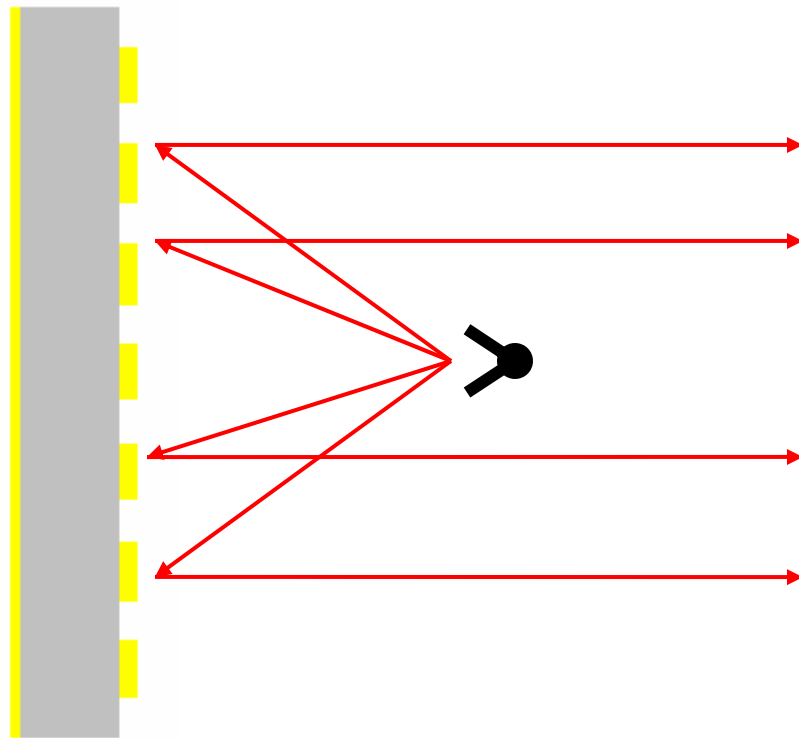


*Figure 1.3: Planar Reflectarray Exhibiting a Parabolic Geometry*

The first reflectarray design published in 1963 was not a microstrip array, but instead relied on an externally illuminated series of stacked rectangular waveguides to impress reflected phase responses [1.15]. Nearly a decade later, in the late 1970s, initial

work began to adapt reflectarray concepts to exploit the emerging field of microstrip technology - giving birth to the modern reflectarray [1.16]. The majority of these early microstrip reflectarrays utilized printed dipole or crossed dipole array layouts for phase modification due to their relative ease in characterization and fabrication. Around the 1990s, more complicated and efficient element geometries emerged with the creation of ring [1.17], variable patch [1.18], and stub-tuned reflectarrays [1.19]. State of the art reflectarray research has begun to focus on reflectarray bandwidth improvement, polarization control, and offset feed configurations.

Several commercially available reflectarrays have already been released to the market. Malibu Research, based in Camarillo, California, currently sells a reflectarray known as FLAPS™ (Flat Parabolic surface) for use in RF and millimeter radar applications [1.20 – 1.21]. The FLAPS™ is an integral component of many new electronic warfare devices including the newly deployed crowd control RF gun. Because the FLAPS™ is designed to be foldable, it allows the RF gun to be rapidly deployed on military or civilian vehicles, unlike earlier designs that utilized bulky reflectors. ILC Dover based in Frederica, Delaware markets an inflatable reflectarray as a way to lower payload weight when deploying in Ka and X band satellite applications [1.22]. Additionally, TRILabs in Canada offers a tunable reflectarray design for beamsteering and offset feeding applications [1.23].

### **1.3 Statement of Thesis**

While reflectarray technology has rapidly matured at both RF and millimeter wavelengths, no public publications are currently available to the author implying on-

going reflectarray research at higher frequencies including short wave millimeter wave, infrared, or visible. In principle, existing reflectarray technology can be simply scaled for use at these higher frequencies; however, the transition is complicated with the appearance of dispersion in fabrication materials, the need for new fabrication techniques and procedures, and considerably higher tolerances in fabrication dimensions.

Additionally, while most RF and millimeter wave reflectarrays traditionally contain only a few hundred elements, small frequency reflectarrays require over one million elements to be practically implemented, simply to overcome the difference in wavelength. The purpose of the thesis is to verify, both experimentally and through modeling, that a sub-millimeter and infrared reflectarray, or SMIR, is feasible by demonstrating that phase variation across a groundplane backed, physically flat surface has been achieved simply by varying the element dimensions of an array on that surface. The thesis will specifically focus on development process of a proof of concept reflectarray at long-wave infrared (LWIR).

#### **1.4 Infrared Reflectarray Development Motivation**

Currently, one of the largest monetary costs associated with infrared optical systems can be attributed to the system's optical components. Previously one of the lower cost items in an infrared system, detector and microchip technology have made great strides in both performance and cost, while traditional optical elements have remained relatively static – with little future advances predicted. Reflectarray technology is desirable to help reduce the cost of some optical elements by replacing costly polishing or diffractive element fabrication with standardized and efficient micro-lithography



techniques. Mass production with lithography is already carried out with most integrated circuit fabrication processes with very little influence on the circuit cost and conceivably reflectarrays could be made using a similar die process. Furthermore, lithography, especially optical lithography, is highly repeatable which would reduce testing and characterization costs.

Lithography is also desirable as it grants additional control to the optical system designer for element specification. With the use of a computer aided design program, it will be possible create a wide variety of arbitrary reflector geometries to meet specific design requirements that cannot be achieved easily or cheaply using conventional polishing techniques. Similarly, the potential ability to control the reflectarray with a high degree of flexibility will be a boon for direct aberration correction and characterization.

Additionally, reflectarray technology integrates desirably with ongoing research into miniaturization and disposable optics. For example, a great deal of effort has been recently placed in miniature unmanned aerial vehicle research (UAV). Reflectarray technology could be easily integrated into UAV devices to reduce the physical footprint of the optics in size and weight and has the additional benefit of being conformal.

## CHAPTER 2: FUNDAMENTALS OF REFLECTARRAY DESIGN

### 2.1 The Variable-Patch Reflectarray

As mentioned from section 1.3, several reflectarray layouts have been designed, fabricated, and tested in the past. Based on this prior research, variable-patch reflectarray designs (Figure 2.1) have gained popularity as the optimal reflectarray element for efficient, wideband applications. Specifically, variable-patch reflectarrays achieve phase shift variation upon reflection by simultaneously varying the length and width of a patch to vary the surface impedance at the element's location on the array. Pozar carried out the initial development of the variable-patch reflectarray [1.18] and several other individuals and organizations have tested and developed similar designs [2.1 – 2.3].

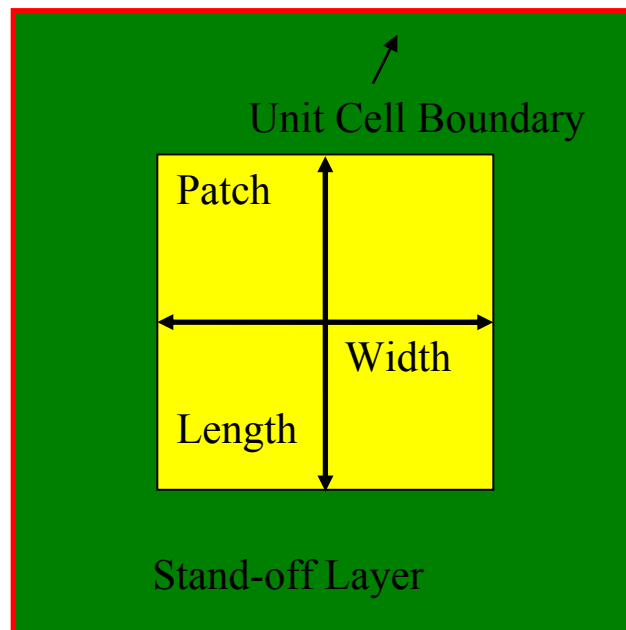


*Figure 2.1: Variable-Patch Reflectarray Layout*

Variable-patch reflectarrays have numerous advantages when compared to other available reflectarray geometries [2.4], which make the design highly desirable for deployment at higher frequencies. Unlike ring element designs, the square patch reflectarray is easily fabricated with a high degree of accuracy using most micro-lithography techniques. The size of the patch scales well with frequency as opposed to reflectarray elements that utilize stubs to generate phase delays. By changing length of the patch independently from the width of the patch element, it is possible to impose phase delays in orthogonal directions for polarization selectivity [2.5]. Most significantly, variable-patch reflectarrays demonstrate superior bandwidths, approaching 10%, - far larger than almost all other single layer reflectarray designs [2.6].

## **2.2 Circuit Equivalent Design: The Transmission Line Approach**

The simplest approach to characterize the behavior of a variable-patch reflectarray is to break up the patches into individual, isolated unit cells and employ an equivalent circuit approximation. Inherently a resonant structure, scattering patches are best represented as a resonating transmission line (Figure 2.2). Beginning at the termination of the transmission line, the reflectarray groundplane will behave as a short, which exhibits a reflection coefficient of -1 corresponding to the expected 180 deg phase shift upon reflection by a plane wave impinging on a perfect electric conductor (PEC) surface. The substrate of the reflectarray can be modeled as the transmission line itself by neglecting any type of dielectric loss. Therefore, the stand-off layer transmission line will exhibit a characteristic impedance equal to the wave impedance of the substrate material ( $Z_d$ ) and with length equal to the height of the substrate ( $d$ ). Assuming the width and length of the

patch are equal, the patch itself can be represented as a variable inductor [2.7], with inductance (L) proportional to the ratio of the area of the patch ( $l^2$ ) relative to the area of the unit cell (A) as demonstrated in Eq. 2-1.

$$L \propto \frac{l^2}{A} \quad \text{Eq. 2-1}$$

Thus, when the area of the patch approaches zero, the inductor will behave as open and when the area of the patch approaches the area of the unit cell, the inductor will behave as a short as expected. The unit cell is finally connected to the open terminals of an infinite waveguide with characteristic impedance equal to the free space wave impedance as a representation of the air above the reflectarray.

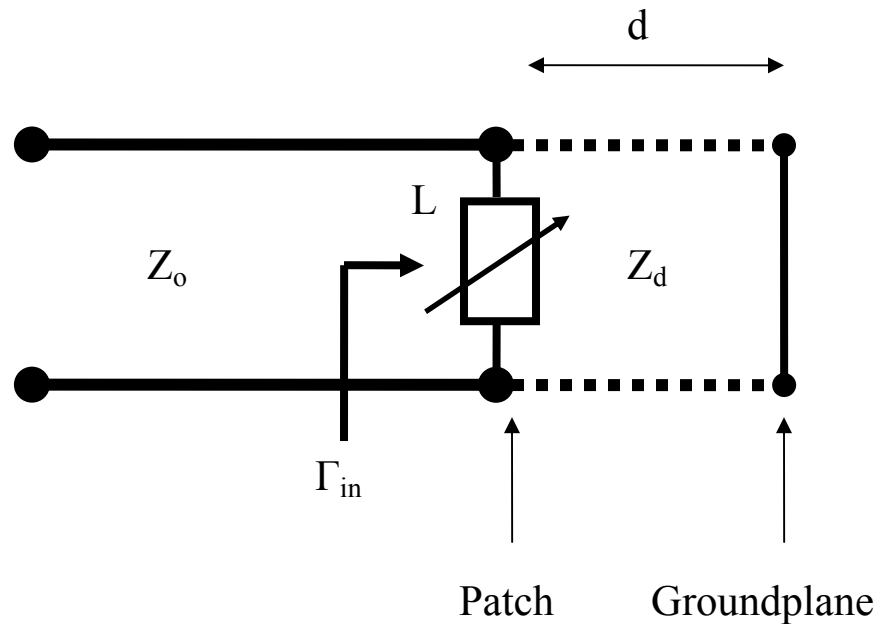


Figure 2.2: Reflectarray Transmission Line Equivalent

Determination of phase shifting can be directly calculated by finding the input reflection coefficient at the interface of the substrate transmission line to the air transmission line. Using conventional transmission line calculations, the reflection coefficient ( $\Gamma_{in}$ ) is represented by

$$\Gamma_{in} = \frac{Z_{in} - Z_0}{Z_{in} + Z_0} \quad \text{Eq. 2-1}$$

where the input impedance ( $Z_{in}$ ) is equal to

$$Z_{in} = \left( \frac{-j}{\omega L(l^2, A)} + \frac{-j \cot\left(\frac{2\pi\sqrt{\epsilon_r}d}{\lambda_0}\right)}{Z_d} \right)^{-1} \quad \text{Eq. 2-2}$$

where  $\lambda_0$  is the free space wavelength,  $\epsilon_r$  is the real part of the substrate's dielectric constant, and  $\omega$  is the free space angular frequency. Finally the phase response of the reflectarray can be calculated by finding the phase of  $\Gamma_{in}$ , or

$$\angle\Gamma_{in} = \tan^{-1}\left(\frac{\text{Im}(\Gamma_{in})}{\text{Re}(\Gamma_{in})}\right) \quad \text{Eq. 2-3}$$

The transmission line model allows for several significant conclusions about the general behavior of the variable-patch reflectarray. First, the height of the substrate will determine the extent of the phase shift achievable by the reflectarray by regulating the initial reflectarray phase response when the patch area is not large enough to introduce a significant inductance and only the groundplane is the dominant radiator. This

phenomenon can be visualized by plotting the phase response of the reflectarray on a Smith Chart (Fig. 2.3) starting at the dominate groundplane state and tracing the entire system response as the patch increases in size. When the patch approaches the size of the unit cell, it will begin to behave as a dominant short, independent of the stand-off layer and groundplane. From this behavior, and taking into account no dielectric is entirely lossless, it is important to utilize the shortest possible substrate height to achieve nearly 360 degrees of phase shifting at a single frequency. Another important conclusion is the input impedance will always be purely imaginary and, thus,  $\Gamma_{in}$  will always have a magnitude of unity – signifying no losses in the system as expected in the idealized model. Additionally, the input impedance is dependent on the area of the patch, which will result in a non-linear relationship between the phase response of the patch and the length of the patch.

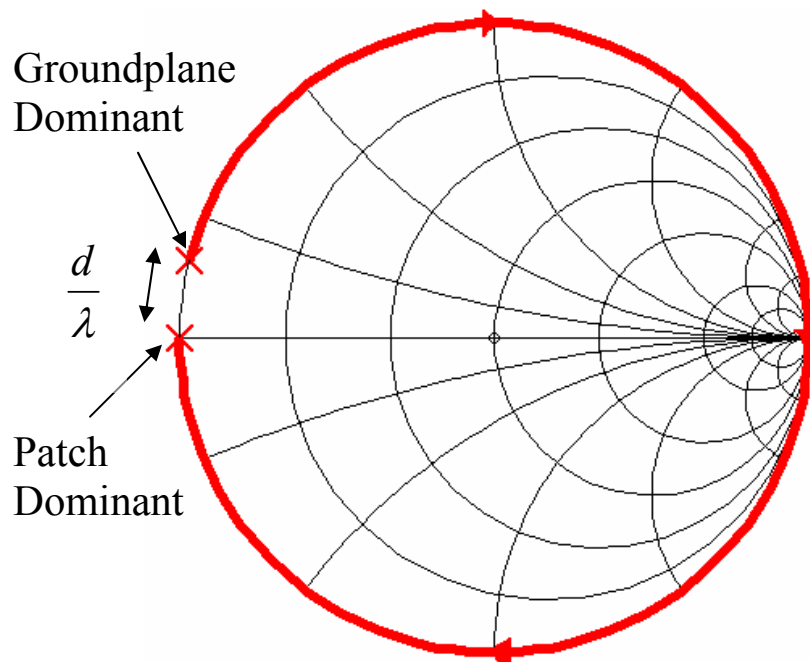


Figure 2.3: Smith Chart plot of  $\Gamma_{in}$  Demonstrating Reflectarray Phase Transition by Varying Patch Size

From Eq. 2-2, the bandwidth properties of a variable size patch reflectarray may also be predicted. If the substrate height is reduced to allow for a larger phase response range at a center frequency, the transformed impedance of the groundplane will decrease to a short as wavelength increases – effectively shorting the patches and preventing operation. If wavelength decreases, the effective dielectric height will increase and the phase response range of the reflectarray will diminish. Additionally, operating bandwidth will not be linearly related to ratio of dielectric height to wavelength.

Although the transmission line equivalent network is highly beneficial for predicting reflectarray behavior, it can rapidly become complex when accounting for system non-idealities such as dielectric or metal losses. Using the physical dimensions of the patch does not correspond to the actual electrical length of the patch that the incoming plane wave will observe sitting upon the substrate due to effective scaling and fringe fields. The model also cannot take into account surface coupling between neighboring elements without the introduction of a correction factor.

### **2.3 Characterization Through Numerical Modeling**

For the highest design accuracy before modeling, most reflectarray designers employ some form of a numerical modeler [2.8]. Numerical modeling takes into account system non-idealities, such as lossy materials or surface coupling, which are difficult to incorporate into the transmission line equivalent without a significant increase in complexity. In the context of the thesis, three independent modeling approaches have been considered and consulted: the single element FEM model, the infinite array FEM model and the Periodic MoM model.

The finite element method (FEM) is a numerical technique by which a three dimensional model, representing the designed antenna, is discretized into a sub-domain in which the fields are represented by local interpolation functions. Matrix equations are derived from a global assembly of the finite elements in the mesh while enforcing boundary conditions. Solving yields local fields at nodes throughout the mesh, which may be interpolated to arbitrary locations. Post processing computations produce far-field information and scattering parameters. Ansoft HFSS, employed in the thesis for FEM modeling, specifically generates tetrahedral meshing elements and utilizes a three-dimensional design interface for model boundary definition [2.9]. Ansoft HFSS also includes numerous features beneficial to modeling reflectarrays; including automated plotting, wave port and plane-wave excitation, and parametric solution sweeps.

While FEM is suitable for three-dimensional geometries, the Method of Moments (MoM) numerical technique lends itself to planar structures by only meshing the radiating structures. Additionally, the reduced discretization required for MoM leads to shorter solution times when compared to similar FEM models. Considering the reflectarray structure to be entirely planar, the shorter simulation times and spatial simplifications make MoM solvers desirable to model reflectarray structures. By meshing the trace surfaces of a design using a given number of polygons for a set frequency, the method of moments technique is used to solve the mixed-potential integral equation (MPIE) and calculate surface current everywhere on the mesh. The MoM can be broken down into two sections: the basis function and the testing function. Ansoft Designer, the MoM solver utilized in the thesis, uses a zero-order normal element basis function to interpolate the interior current values from values on the edges [2.10]. Zero-order normal



elements have one unknown for each edge in the mesh. Testing functions are applied to the MPIE to obtain a matrix equation, which is then solved to find surface current. From the surface current, Designer calculates the S-parameters and the radiated fields. Much like Ansoft HFSS, Designer also includes support for finding far fields, plane wave excitation, and parametric solving.

### **2.3.1 Finite Element – Single Element Modeling**

Of the three models, the Single Element FEM model requires the least effort to design at the cost of the potential for over-simplification [2.11]. The basis for the validity of single element FEM model is from research that suggest shorted antenna elements, or antenna elements above a groundplane with an electrically thin stand-off layer, will experience very little coupling between neighboring elements [2.12]. Therefore, this assumption allows reflectarray patch elements to be modeled as single elements for accurate characterization of phase behavior without taking into account the influence of neighboring elements.

Creation of a Single Element FEM model (Figure 2.4) follows the standard procedure used in the formulation of any HFSS antenna model. The foundation of the model is a three dimensional rectangle representing the stand-off layer with assigned thickness and dielectric properties representing the desired fabricated values. Similarly, the rectangle will have length and width equal to the spacing of a single reflectarray unit cell. A two-dimensional rectangular PEC boundary sits on the top face of the substrate to represent the variable size patch. A three-dimensional air box wraps around the substrate to bound the entire model space with the bottom face of the air box touching the bottom

face of the stand-off layer. Radiation boundaries exist on each of the sidewalls of the air box and, on the bottom face of the air box, a PEC boundary represents the reflectarray's groundplane. Finally, the top of the air box terminates with an excited wave port set with intrinsic impedance matched to the wave impedance in air. Solving the model occurs by varying the size of the rectangle representing the patch and calculating the change in reflection phase at the wave port.

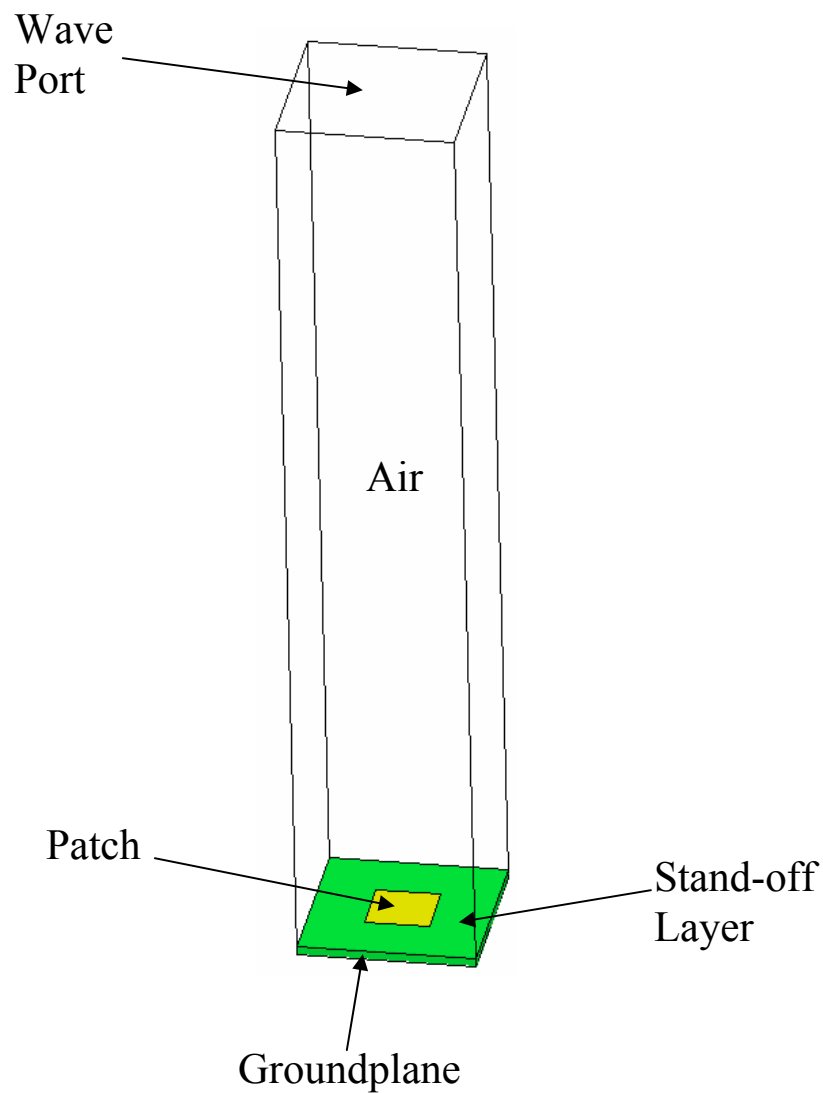


Figure 2.4: Model Layout for FEM Single Element Reflectarray Modeling

### **2.3.2 Finite Element – Infinite Element Modeling**

The Infinite Element FEM (Figure 2.5) modeling approach attempts to reduce the number of potentially inaccurate assumptions made in the Single Element FEM modeling approach at the cost of additional complexity. Starting with the Single Element model, the top boundary air box is replaced with a radiation boundary and the model is excited by a uniform plane wave. Fields radiated by the wave port will not be planar or uniform and the addition of the plane wave excitation establishes more realistic model parameters. Instead of radiation boundaries, the sidewalls of the model have defined Master/Slave boundaries. Master/Slave boundaries are linked boundaries where field patterns exiting one boundary are forced to match patterns entering on the other boundary. The purpose of such a boundary is to account for coupling between neighboring elements, both in the dielectric and in the air, commonly seen in phased array designs. Similar to the Single Element model, solving occurs by varying the patch size and finding the change in the far-field phase.

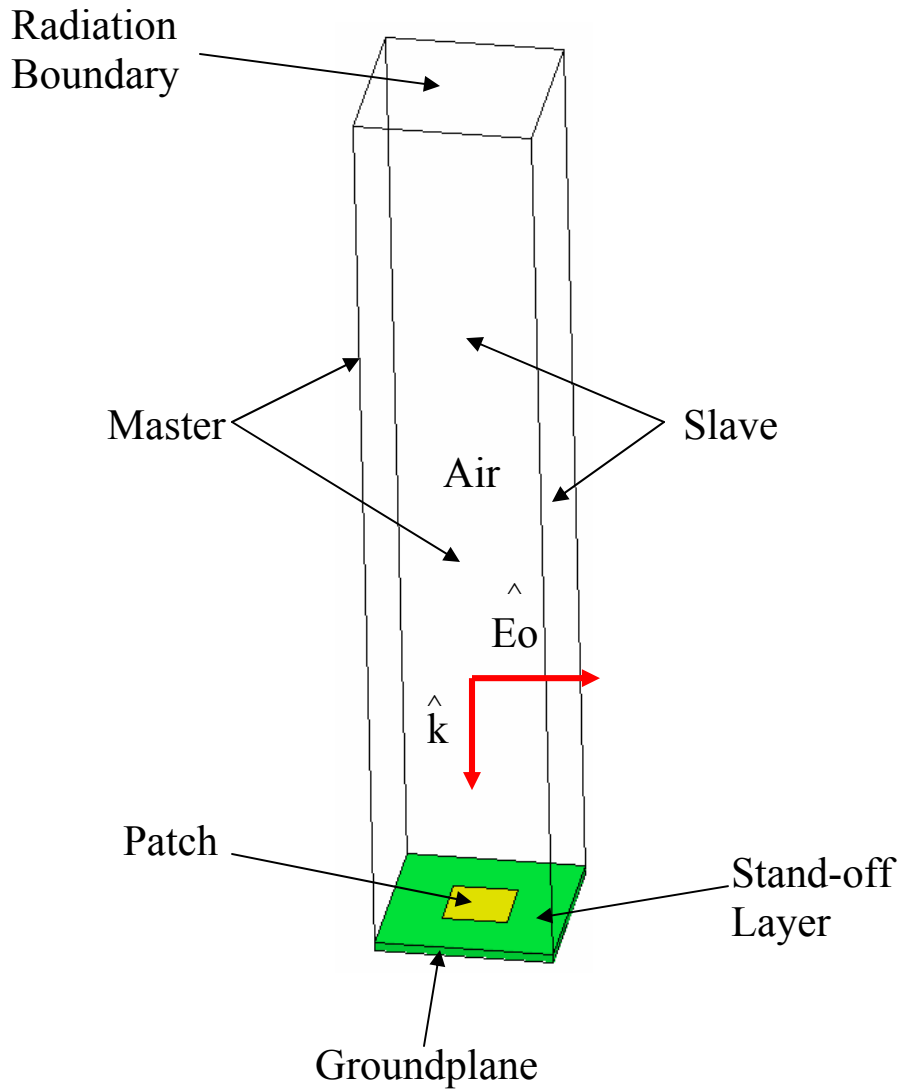
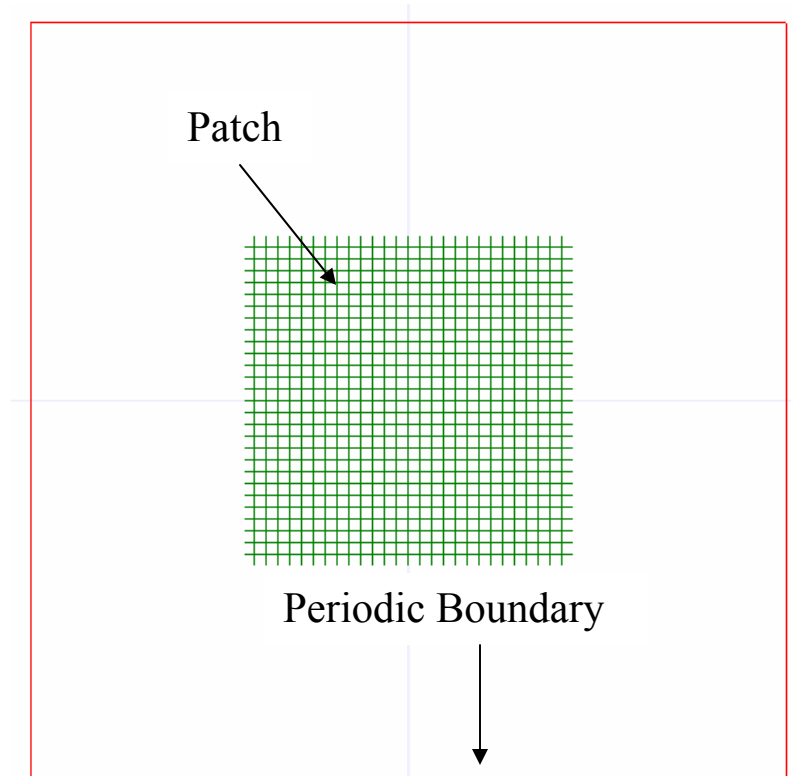


Figure 2.5: Model Layout for FEM Infinite Array Reflectarray Modeling

### 2.3.3 Periodic MoM Modeling

Unlike HFSS, in the Periodic MoM model in Ansoft Designer there is no need to specify the three dimensional geometries, but a layer stackup is utilized (Figure 2.6). Through the layer stackup, Designer defines thickness and material properties for the stand-off layer, groundplane, and trace layers. Within the trace layer, a square represents

the patch element. To take into account coupling between neighboring elements, the edges of the model have periodic boundary with size equal to the periodicity of the array. Excitation is a plane wave at normal incidence. Far-field phase is found by varying patch size and calculating the phase change of the reflectivity.



*Figure 2.6: Model Layout for Periodic MoM Reflectarray Modeling*

## CHAPTER 3: DEVICE SIMULATION AND MODELING

### 3.1 Initial Device Specification

Before modeling began, initial reflectarray design parameters were specified. Based on measured ellipsometric data from the IR Systems Lab at the University of Central Florida [3.1], Zirconium Dioxide ( $ZrO_2$ ) was chosen to be best suited for use as the reflectarray's substrate due to the materials reasonable loss and low permittivity at 28.3 THz when compared to other common dielectrics such as Silicon Dioxide or Silicon Nitride. As a passive device, low loss in the dielectric making up the stand-off layer is highly desirable for encouraging high overall system efficiency. With a dielectric constant of approximately 2.0, effective scaling of the patches is reasonable compared to other dielectrics used in IR antenna fabrication, which reduced fabrication tolerances and reduces the number of elements to achieve proper reflectarray behavior.

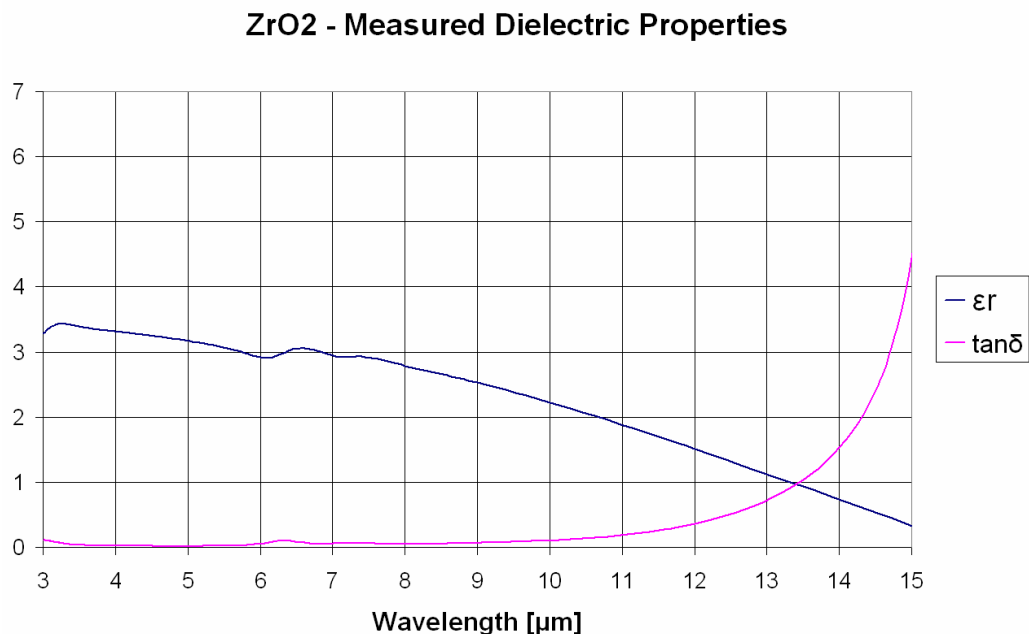


Figure 3.1: Measured Dielectric Properties for  $ZrO_2$

Patch spacing approximately equal to the center-operating wavelength, in the dielectric, traditionally allows for optimal variable-patch reflectarray performance [1.18]. Again for a device designed for operation at a free space wavelength of 10.6  $\mu\text{m}$  using a  $\text{ZrO}_2$  stand-off layer, element spacing was chosen to be 5.54  $\mu\text{m}$ . For the stand-off layer height, one-sixteenth the center operating wavelength, in the dielectric, satisfies isolation conditions and will limit losses in the dielectric; however, due to fabrication limitations the fabricated reflectarray utilized a stand-off height of 450 nm, approximately one twelfth of the wavelength.

**Table 3.1: Initial Model Specifications**

<b>Specification</b>	<b>Value</b>
Element Spacing	5.54 $\mu\text{m}$
Dielectric Material	$\text{ZrO}_2$ ( $\epsilon_r = 2.0$ $\tan\delta = 0.15$ )
Dielectric Height	450 nm

### **3.2 Reflectarray Simulation Results**

The modeling procedures in section 2.3 were employed to analyze the proposed reflectarray structure and both the Infinite Array FEM model and the Periodic MoM model exhibited mutual agreement and correspond well to previously published results. From the two models, patch size ranges were then predicted for use in fabrication. The patch size selection process for the SMIR proof of concept is further discussed in section 4.3. The Single Element FEM model; however, did not correspond well with the other two models or prior measured data and was not used in designing the fabricated SMIR. The results from the three models are plotted together for comparison in Figure 3.2.

### Phase Response Comparison

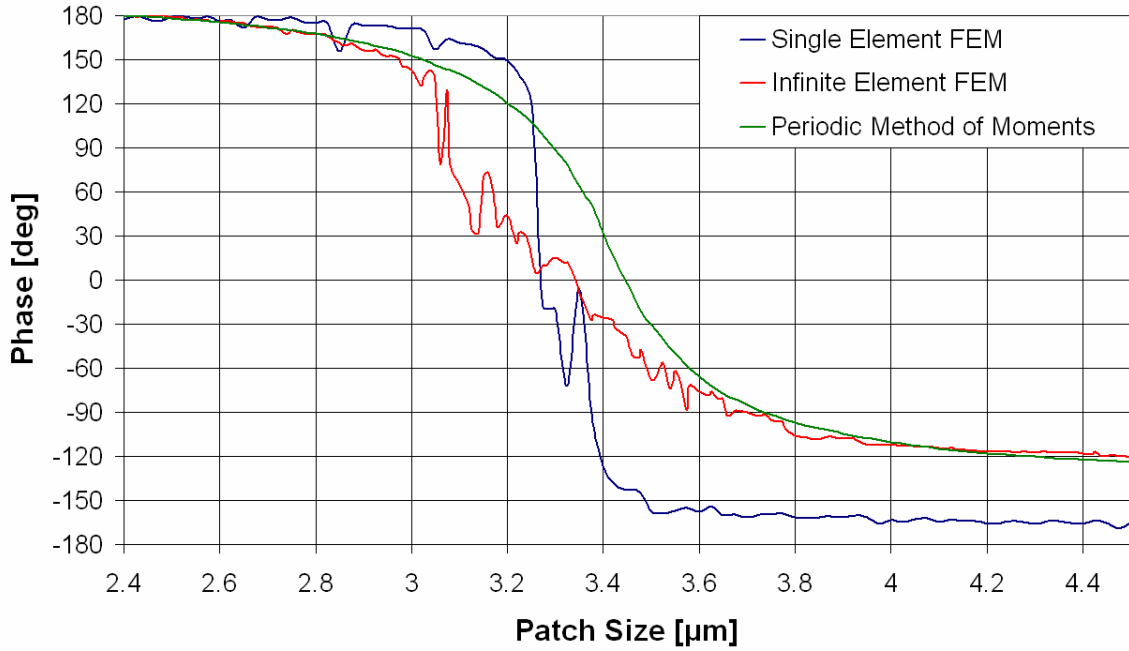


Figure 3.2: Comparison of Modeled Results



## CHAPTER 4: DEVICE FABRICATION

### 4.1 Device Layout

To physically test the feasibility of an IR reflectarray, a simple two inch, three stripe reflectarray was developed (Figure 4.1). Three 0.25 inch by 1.09 inch wide arrays of patches, isolated from each other on the dielectric by 0.3125 inch, was deposited on a groundplane backed stand-off layer for testing. Each uniform array was made up of a single sized patch element to demonstrate a unique phase shift upon reflection for comparison to prior modeled results. In addition, an optical flat was used as the devices substrate to ensure that any phase modification occurs due to the patches only and not due to a physical defect in the substrate.

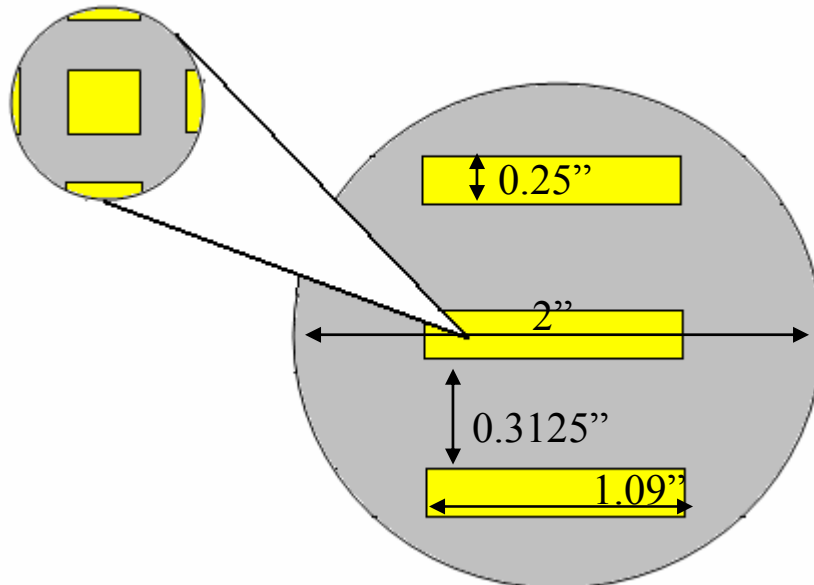


*Figure 4.1: Proof of Concept SMIR Layout*

## **4.2 Fabrication Methodology**

Prior to device fabrication, an adequate substrate was selected to meet the specifications of the equipment used in IR antenna fabrication, which typically requires substrates of no greater than a few millimeters thick. To insure proper flatness and avoid flexing of the substrate; however, most optical flats require thicknesses comparable to the diameter of the substrate. For the SMIR, a 0.125 inch (3.175 mm) thick, quarter wave optically flat fused silica substrate was determined to be the thinnest two inch optical flat commercially available. Although relatively thin, the optical flat is 8 times thicker than the silicon substrates traditionally used in IR fabrication. The increase in substrate thickness demanded additional investigation and modification of conventional fabrication processes used in the lab.

Before fabrication of the reflectarray patch stripes, the groundplane and substrate was deposited. Substrate deposition on the optical flat for the proof of concept devices was carried out by an external company, Evaporated Coatings, Inc. in Willow Grove, PA. A 200 nm thick layer of gold was evaporated onto the provided optical flat to act as the SMIR's groundplane. To aid in gold adhesion to the fused silica, 20 nm of titanium was first deposited on the bare flat. The adhesion layer is necessary, as gold will not adhere to surfaces with native oxide layers without an adhesion layer or removal of the oxide layer through etching. Although restricted in use by the need of an adhesion layer, gold is desirable for the SMIR groundplane due to the fact it has one of the highest conductivities of any metal at infrared frequencies and will not corrode or form a native oxide layer. From prior measurement, the adhesion layer is determined to be optically thin enough not to have a significant impact on the performance of the device. Similarly,

a second 5 nm titanium layer was deposited on the exposed gold layer to ensure adhesion between the groundplane and stand-off layer. Finally, a 450 nm layer of  $ZrO_2$  was deposited on the groundplane and the coated flat (Figure 4.2) was returned to the University of Central Florida for pattern writing.

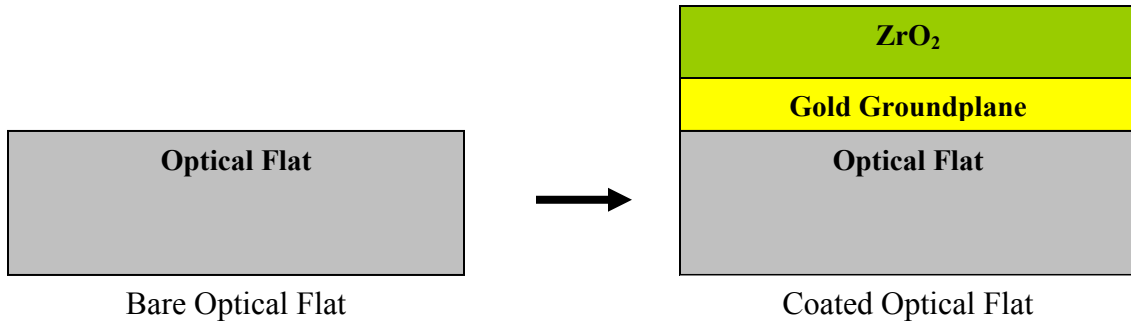


*Figure 4.2: Optical Flat Coating Process*

Pattern writing of the SMIR followed a standardized e-beam fabrication procedure developed by Charles Middleton, a member of the IR Systems Laboratory at the University of Central Florida. For the proof of concept devices, pattern lithography was carried out using an e-beam lithograph system. Due to the modeled minimum feature size of the reflectarray, alternative fabrication techniques could be used at a lower cost and are discussed in section 6.2.2 of the thesis; however, e-beam lithography allowed for fabrication with the highest confidence in accurate element dimensions desired in the initial proof of concept phase of the research. E-beam lithography utilizes a scanning electron beam to write a desired device pattern into an e-beam sensitive resist made up of large chains of polymers deposited on the device's stand-off layer. When exposed to an electron beam, the polymers in the resist break apart and, in the case of positive resist, the exposed region can then be removed from the surface of the stand-off layer using a

chemical developer. The size and sharpness of the uncovered pattern is controlled by the electron beam current, dose, and size, which requires prior characterization. With the desired regions of the stand-off layer exposed, it is possible to deposit the metal making up the patches using a conventional e-beam evaporation process. Because the evaporation process deposits metal uniformly across the wafer, a final lift off process is necessary to remove undesirable metal deposited on the resist and the remaining resist itself.

Before fabrication begin, the coated optical flat was cleaned to remove any organic or large particles on the coated surface that may contaminate the fabrication process. The wafer was spun at 6000 RPM for one minute and was sprayed for 10 seconds each with Acetone, Methanol, and Isopropyl Alcohol (IPA), in that order. The coated flat was then placed on a hotplate at 180 °C for dehydration baking. After three minutes, the flat was removed and blown for ten seconds using nitrogen to remove any particles that may have accumulated on the surface of the wafer during baking. To ensure an optimal lift-off, a bi-layer positive resist structure was then spun onto the coated side of the optical flat. Initially, PMGI SF7 was spun on at 3000 RPM for 80 seconds and baked for three minutes at 180 °C for a layer thickness of about 400 nm. Next, ZEP 520A-7 was spun on the PMGI layer at 3000 RPM for 80 seconds and baked for four minutes at 180 °C for a layer thickness of about 300 nm.

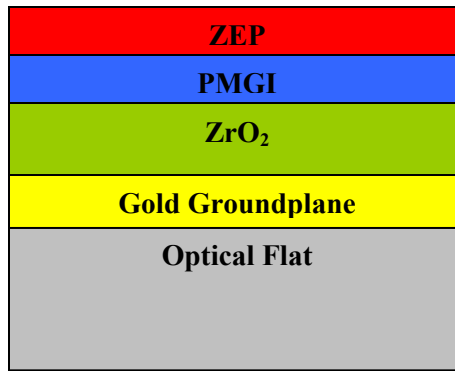


*Figure 4.3: Bi-layer Resist*

The UCF/CREOL Leica EBPG5000+ Electron Beam System, the system used for pattern writing of the SMIR design, is designed to only support substrate thicknesses of up to 3 mm, smaller than the thickness of SMIR optical flat. To overcome this limitation, a region in the e-beam's mask holder was located, which would allow the optical flat to lie recessed, without risk of damaging the e-beam system. A 5-inch mask was machined with a 2 inch lipped hole dropped below the top face of the mask by 0.125 inch (Figure 4.4). Two gold clips were added on opposite sides of the hole to ground the substrate and prevent the groundplane from charging. The resist-coated wafer was then loaded into the holder, held in place by the two clips, and loaded into the Leica EBPG5000+ for vacuum pump down. Pattern exposure for the reflectarray lasted for approximately two and one half hours, upon which the exposed wafer was removed from chamber, ready for development.

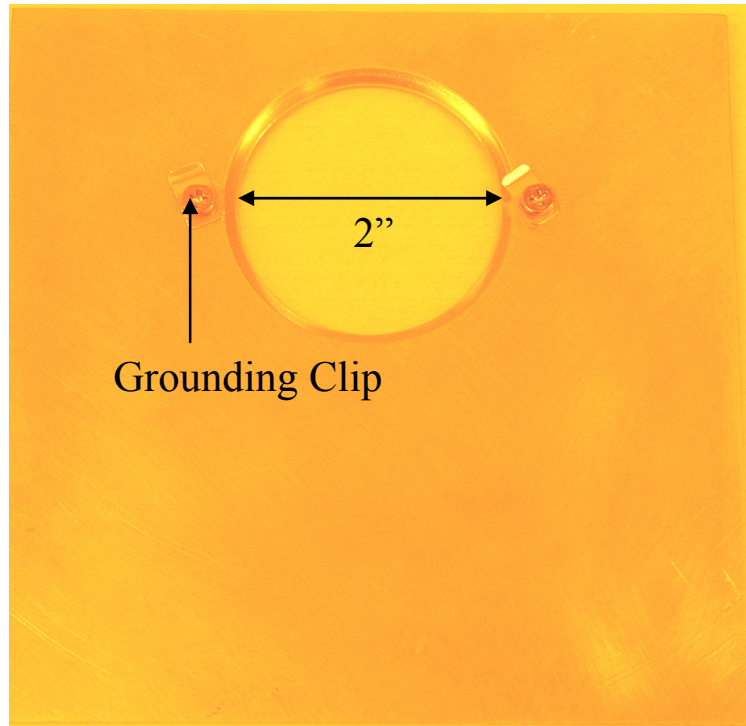


*Figure 4.4: SMIR E-Beam Holder*

Development of the resist bi-layer is a two-step process (Figure 4.5). The exposed ZEP layer was developed and removed by bathing the wafer in ZEP RD developer for 90 seconds. Development was then stopped by an IPA rinse and the wafer was dried using nitrogen. The exposed PMGI layer was developed by using MF 701 developer for 20 seconds. Development of the PMGI layer was stopped by a water rinse and the wafer is dried again using nitrogen. In the ZEP Layer, the desired patch pattern is well defined, with smooth sidewalls, but, due to a partial etching process, the PMGI layer will exhibit bell shaped sidewalls. The curved shaped sidewalls are important to reduce the risk of overlap between metal on the top of the resist and the bare wafer during the e-beam evaporation process. If the two layers do come in contact, it is possible that liftoff of the gold from the resist will also rip off the desired gold making up the patches.

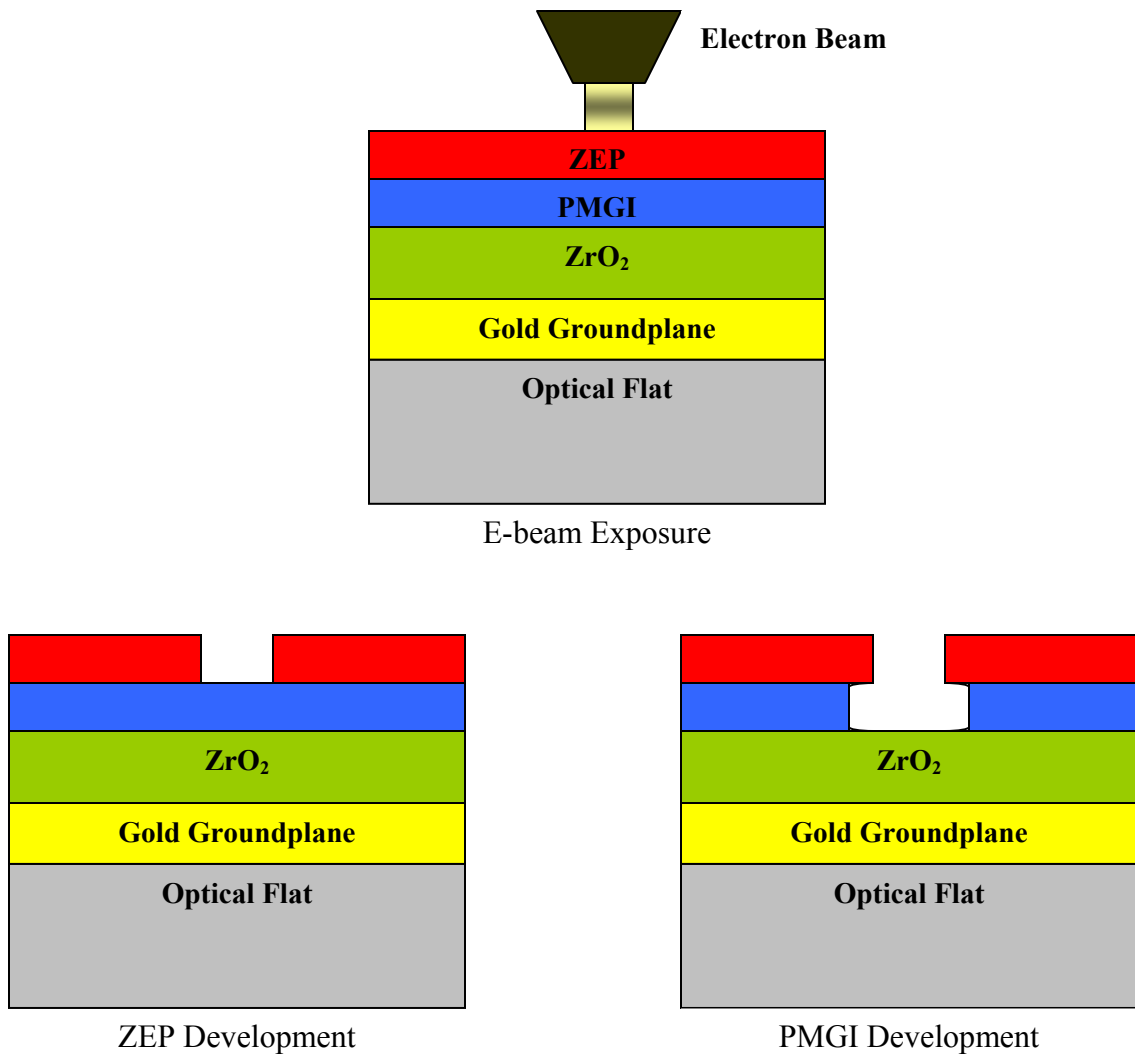


*Figure 4.5: E-Beam Development Process*

The developed wafer was then loaded into an e-beam evaporator. Similar to deposition process used in depositing the groundplane, a 150 nm gold layer, with a 10 nm titanium adhesion layer, was evaporated onto the wafer. The final lift-off process was employed to remove the unwanted deposited metal and un-developed resist. The gold layer was first removed by gently rolling scotch tape across the entire wafer due to poor adhesion between the metal and the ZEP resist layer. The ZEP layer was then lifted-off in a methylene chloride ultrasound bath and, subsequently, excess methylene chloride was removed with an IPA rinse. The remaining PMGI layer was removed using EBR PG

remover and the wafer was once again rinsed with IPA. At this point, only the desired gold patch pattern remained and the SMIR was ready for testing.

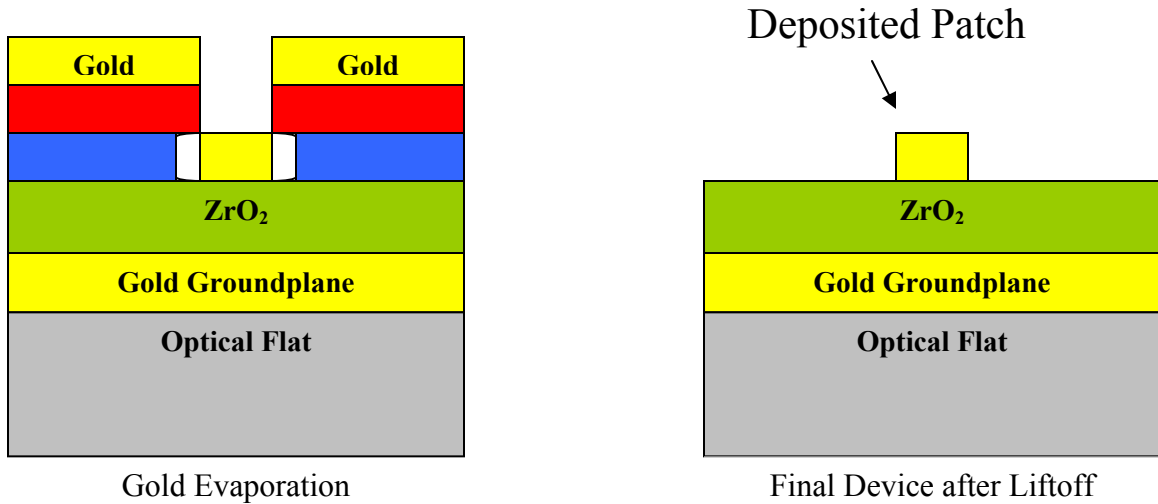


Figure 4.6: Evaporation and Lift-off

### **4.3 Fabricated Devices**

Two initial fabrication runs were made to characterize the fabrication process outlined in section 4.2. The first run involved a 4 by 4 dose matrix of arrays consisting of alternating rows of 2.98  $\mu\text{m}$ , 3.14  $\mu\text{m}$ , and 3.24  $\mu\text{m}$  size patches with a fixed periodicity of 5.54  $\mu\text{m}$  (Figures 4.7 and 4.8). The purpose of this run was to determine the necessary dose to achieve well-formed patches, verified by imaging of the device using an scanning electron microscope (SEM). The second run consisted of verifying the desired dose from the first fabrication run using a slightly larger array of patches and did not require metallization. With development complete, it was possible to use a visible microscope to



observe the exposed pattern in the resist and verify that the predicted dose resulted in well-formed patches.

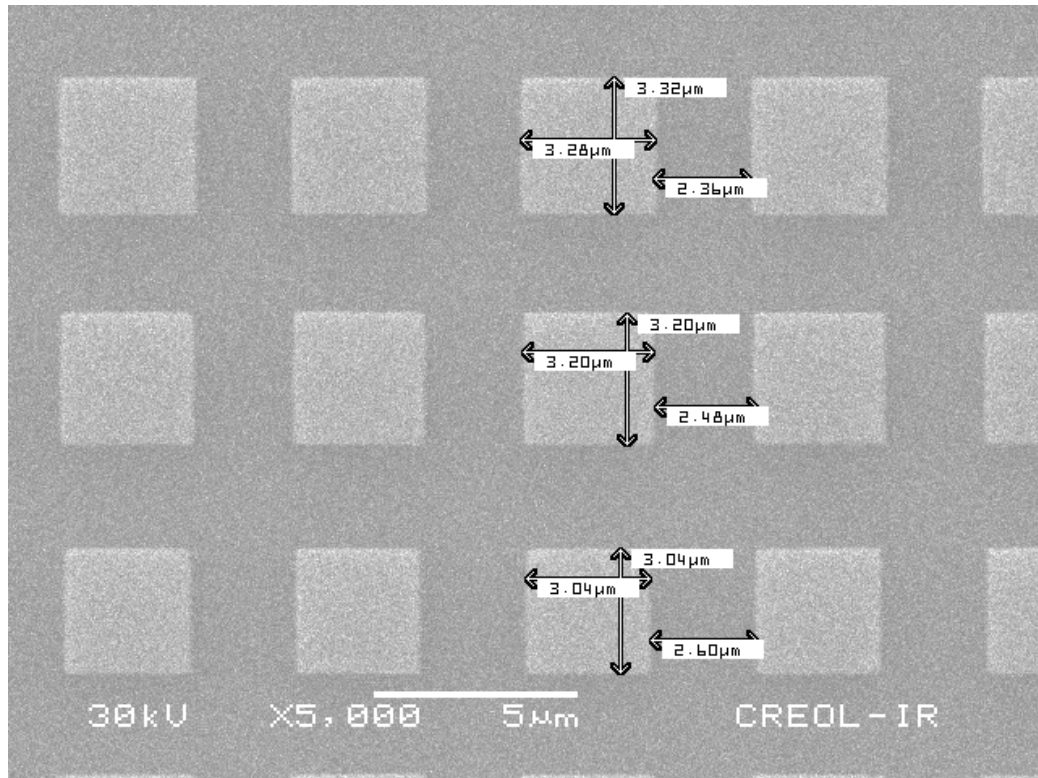
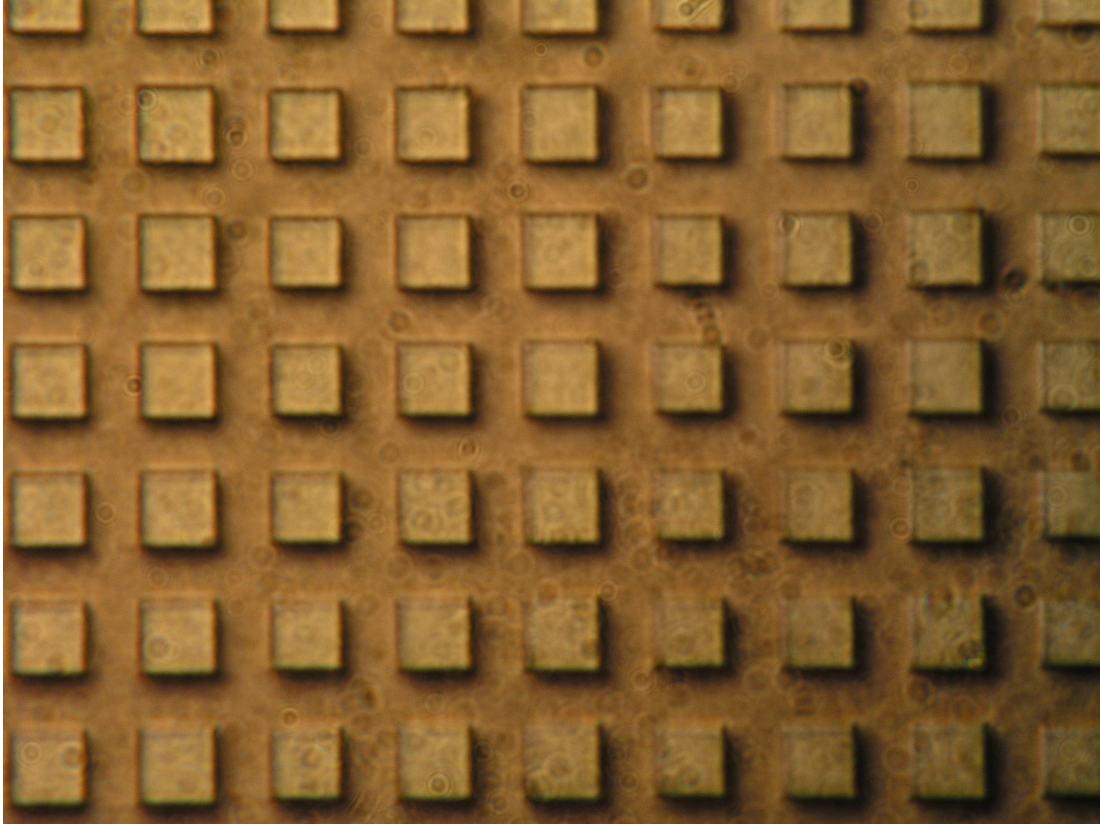


Figure 4.7: SEM image of Metalized Dose Matrix



*Figure 4.8: Visible Image of Metalized Dose Matrix*

For the proof of concept, two devices were fabricated. The first device used the same patch dimensions as the initial dose matrix for three SMIR rows -  $2.98\ \mu\text{m}$ ,  $3.14\ \mu\text{m}$ , and  $3.24\ \mu\text{m}$ . The patch size values were chosen based on averaging the calculated phase responses from Infinite Element FEM model and the Periodic MoM model, which suggested a phase shift of 40, 80, and 120 degrees, respectively (Figure 4.9). The three rows in the second device were chosen blind to the modeled results for the purpose of providing additional sample points in the event that the developed models were incorrect and the patch sizes were measured to be  $2.74\ \mu\text{m}$ ,  $2.84\ \mu\text{m}$ , and  $3.34\ \mu\text{m}$  (Figure 4.10). Unlike the first device, the second fabricated reflectarray suffered several fabrication setbacks, most notably the use of contaminated de-ionized water in development of the PMGI layer. Thus, measured results for the second device was approached with some

caution; however, visual inspection of the reflectarray did not indicate any noticeable flaws. Images of one of the reflectarray stripes for the first device are presented in Figures 4.11 and 4.12.

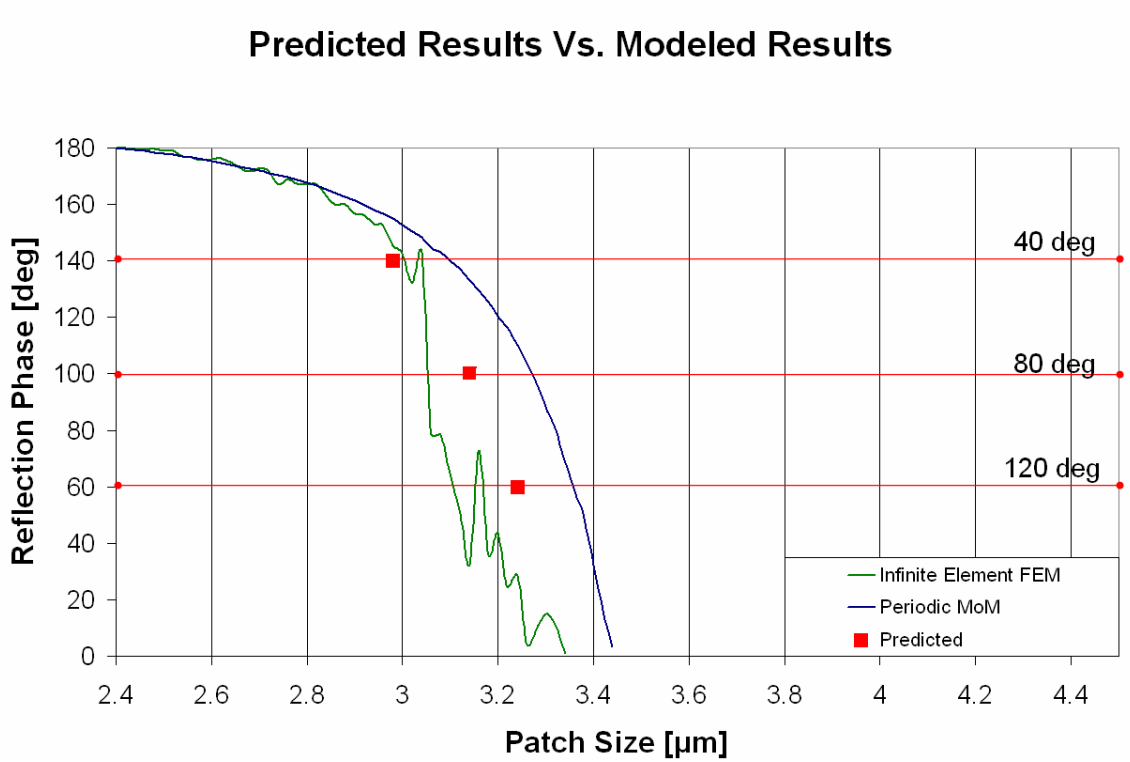


Figure 4.9: Comparison of Modeled and Predicted Phase

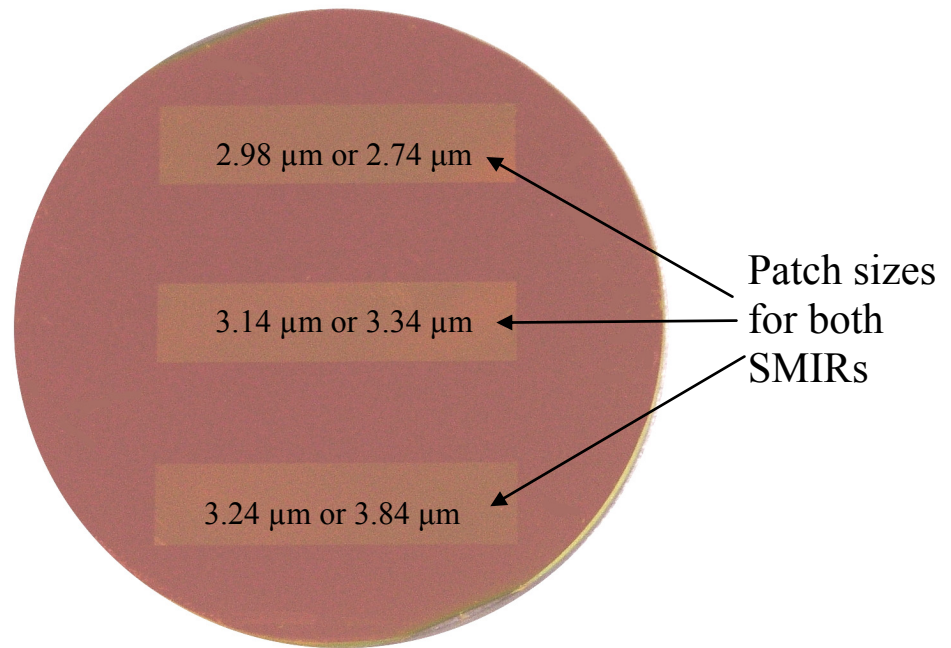


Figure 4.10: Fabricated Strip SMIR with Reference Sizes

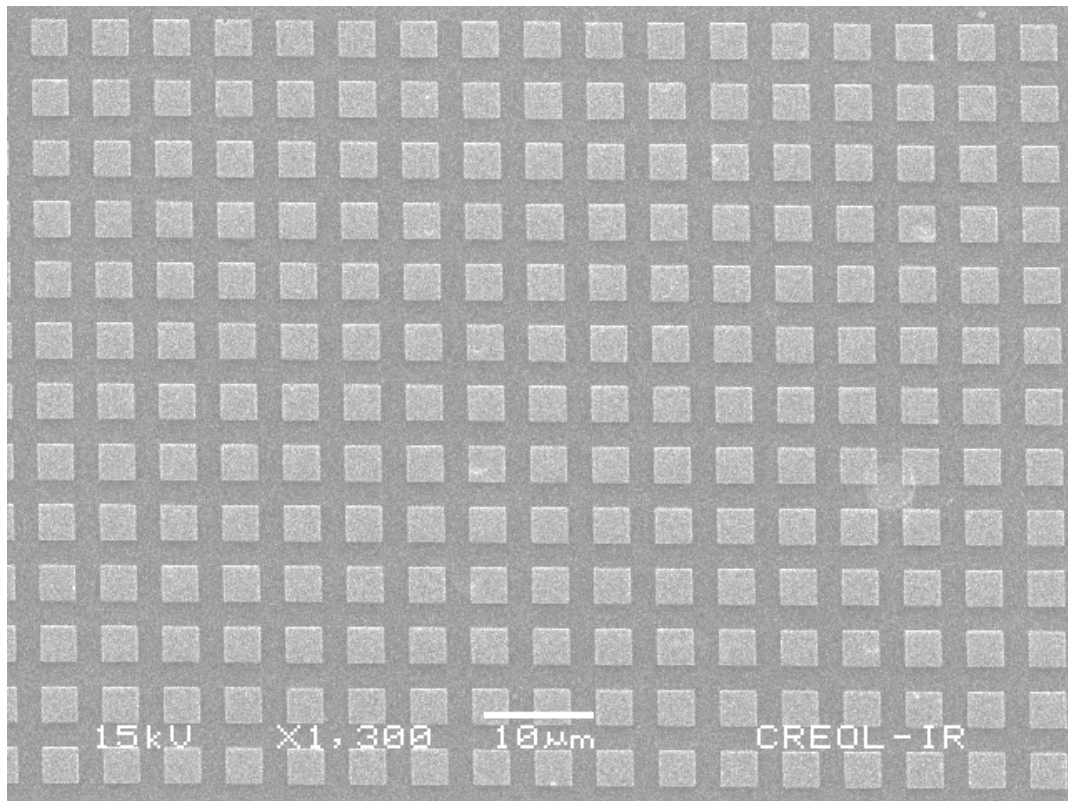
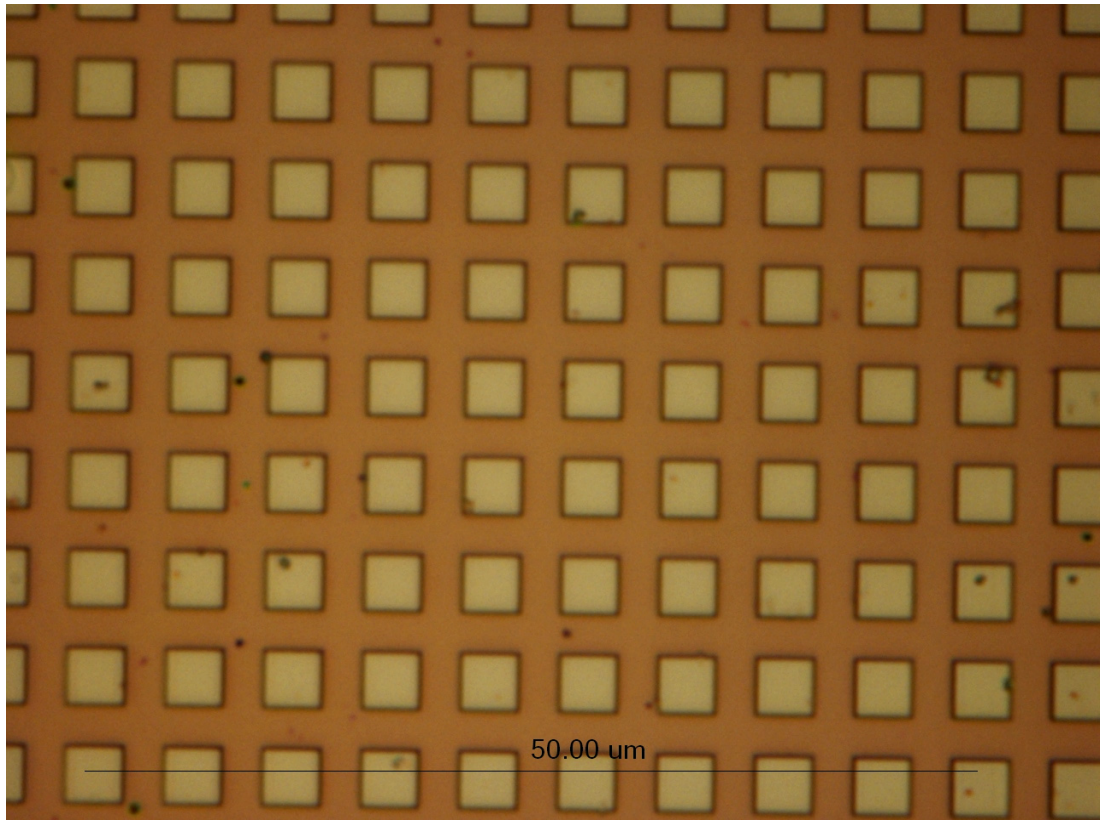


Figure 4.11: SEM Image of One of the Stripes of the Fabricated SMIR





*Figure 4.12: Visible Image of One of the Stripes of the Fabricated SMIR*

## CHAPTER 5: DEVICE TESTING AND RESULTS

### 5.1 Testing Methodology

As stated in the previous chapter, testing of the fabricated SMIR devices was carried out using a 10.6  $\mu\text{m}$  wavelength interferometer. Specifically, the interferometer used in testing was a Wyko IR3 10.6  $\mu\text{m}$  interferometer located at Lockheed Martin Missile and Fire Control in Orlando, FL operated by Lab Engineer Darren Zinn. The IR3 interferometer is a Twyman-Green interferometer, a configuration commonly used in testing of polished optics for design flaws. For a typical Twyman-Green interferometer (Figure 5.1), a coherent light source (for testing of the SMIR devices, a 10.6  $\mu\text{m}$  CO<sub>2</sub> Synrad laser) focused into a pinhole and collimated into a beam splitter. Half of the beam passes through a beam expander and reflects off the test device back into the interferometer. The other half of the beam reflects off a flat reference surface inside the interferometer, typically a gold mirror on a piezoelectric substrate for tilt adjustment and correction. The two beams are then redirected to an IR camera or detector by the internal beam splitter for imaging of the generated interference pattern arising from the test and the reference beams.

## Twyman-Green Interferometer

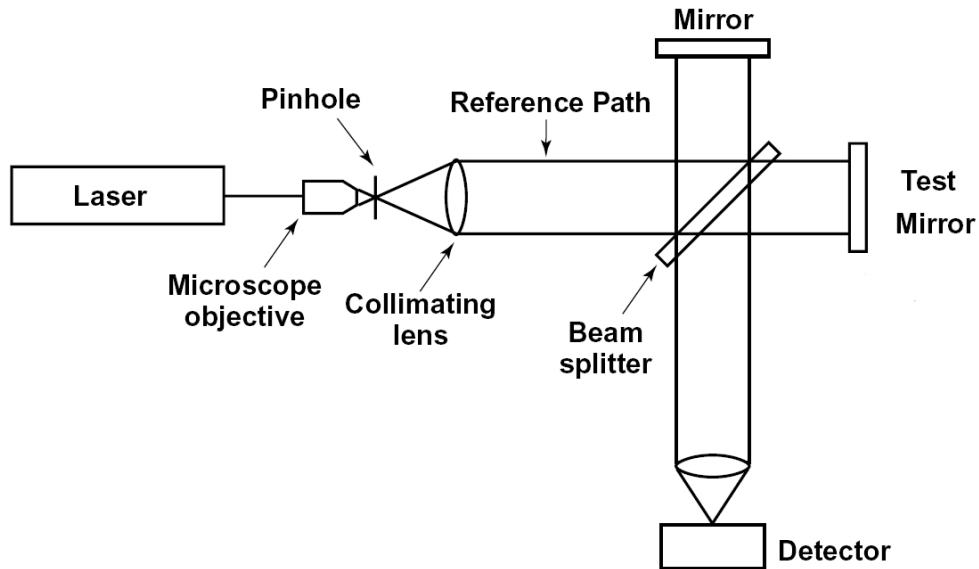


Figure 5.1: Twyman-Green Interferometer [3.1]

The resulting interference pattern can then be utilized to determine surface variations between the device under test and the reference mirror. If an ideal mirror was placed perfectly aligned to the reference mirror, the reference and test beams will arrive at the beam splitter in phase and the detector will image a uniform illumination across the field of view. If the reference mirror or the test mirror were at a slight tilt, a series of bright and light fringes would be imaged, corresponding to the interference resulting from the two beams no longer return in phase due to the path difference introduced by the slight tilt between the two mirrors. Thus, increasing the tilt of the either mirror will increase the number of fringes across test device corresponding to the increased change in path difference across the plane of tilt.

If the test mirror had some physical deformity, such as curvature, the fringes of the generated interference pattern of the tilted mirrors would be shifted to reflect the

difference in path length introduced by the physical height difference arising from the deformity. By measuring the fringe shift relative to its reference, or tilted, position, it is possible to determine the physical height variations across the test device by relating phase difference to path length difference. As such, the Twyman-Green is referred to as a two-pass interferometer due to the fact that a physical height change on the test device will result in a fringe shift in the interference corresponding to twice the height of the deformity (Eq. 5-1). This is a result of the path length for both the incoming wave and reflected wave changing equally by the height change. Therefore, the Twyman-Green can only resolve height differences equal to half the wavelength, otherwise aliasing will occur and the height difference cannot be determined.

$$\theta_{fringeshift} = \frac{2\sqrt{\epsilon_r} height}{\lambda_0} * 360^\circ \quad \text{Eq. 5-1}$$

For testing of the fabricated reflectarray, a similar approach can be used to determine phase shifting by the reflectarray patches. Although the device is physically flat, the phase difference introduced upon reflection will still introduce interference, which can be characterized using the interferometer. For the proof of concept devices, the interference fringes were placed orthogonal to the patch rows and, thus, phase shifting by the reflectarray can be easily measured relative from the regions outside the reflectarray stripes by observing the fringe shifts. Unlike conventional polished optics characterization, however, the interferometer is no longer double pass, as phase shifting occurs upon reflection and does not influence the reflected or incident path length, reducing Eq. 5-1 to 5-2 and allowing for detection of phase shifts greater than 180



degrees. Additionally, it should be noted that the fringe shifting introduced by the patches is linearly shifted compared to reference regions due to the double pass height difference between the groundplane and the patch height.

$$\theta_{fringeshift} = \frac{\sqrt{\epsilon_r} height}{\lambda_0} * 360^\circ \quad \text{Eq. 5-2}$$

## **5.2 Measured Results**

Measured results were images taken by the IR3 IR camera and are presented in Figures 5.2 and 5.3. The first device to be tested was a coated optical flat to verify that the flat did not exhibit any significant physical aberrations because of the substrate and groundplane deposition process. From the measured results, the optical flat exhibits excellent flatness at 10.6  $\mu\text{m}$  that implies that all fringe shifts observed by the interferometer will be entirely a result of the reflectarray. Observation of the two fabricated reflectarrays successfully demonstrate that each row in the reflectarray does in fact demonstrate a unique phase shift and that the phase shift is entirely dependent on the size of the reflectarray patches.

One unavoidable issue that arose from the testing was non-uniform illumination of the device under test. Although present in the testing of the first device, this phenomenon was especially dominant for the second device, which was tested at a later date. The non-uniform illumination was a result of misalignment of the interferometer and not a product of the devices under test. Additionally, this misalignment makes

efficiency characterization with the interferometer impossible and increases the difficulty of post analysis.

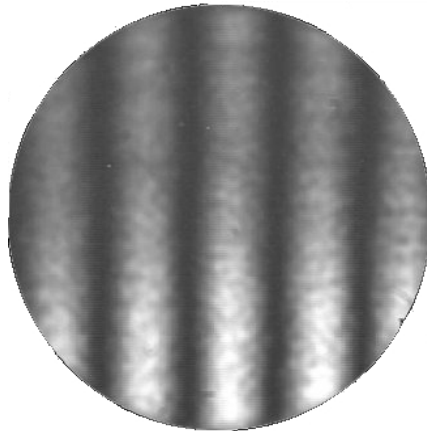


*Figure 5.2: Interferogram of Coated Wafer  
Non-uniform illumination is clearly present, with the bottom of the wafer “hotter” than the top of the wafer*

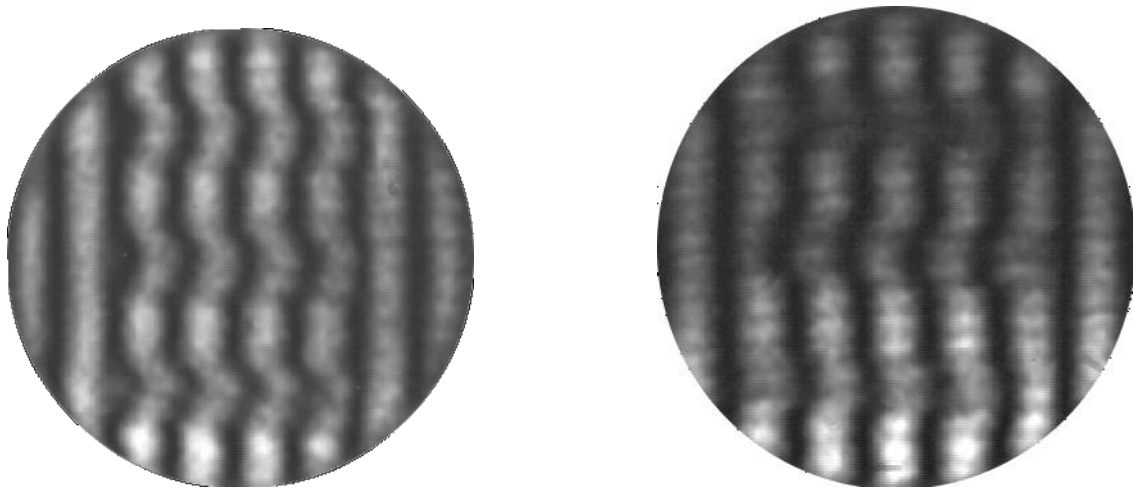


*Figure 5.3: Interferograms of Fabricated SMIRs*

### **5.3 Result Analysis**

With the measured data in hand, it is now possible to begin analysis of the results. For this purpose, two MATLAB functions were written to carry out fringe following. For

both functions, the interferogram generated by the interferometer was read in by the program and converted to an intensity matrix, normalized to account for the non-uniform illumination of the device, and cropped to only contain the center fringes passing over the reflectarray stripes. The first MATLAB function then parsed the intensity matrix locating the center of each bright and dark fringes. With the center positions known, the distance between the maximum and minimum intensities was calculated to find the phase shift relative to the unshifted reference regions on the reflectarray. All of these values are averaged and approximate phase shifts were generated.

The second MATLAB function followed a similar process as the first by initially fitting the dark and light fringes across the reflectarray to a sinusoid. The primary purpose of the fitting was to allow for fringe smoothing and to reduce reflectarray edge noise and non-idealities in the testing setup. Unlike the first function, no averaging was necessary, as the phase shift is optimized as a fitting perimeter for the sinusoid and was directly available. Results from both functions are presented in Figures 5.4 - 5.7 for both fabricated devices.

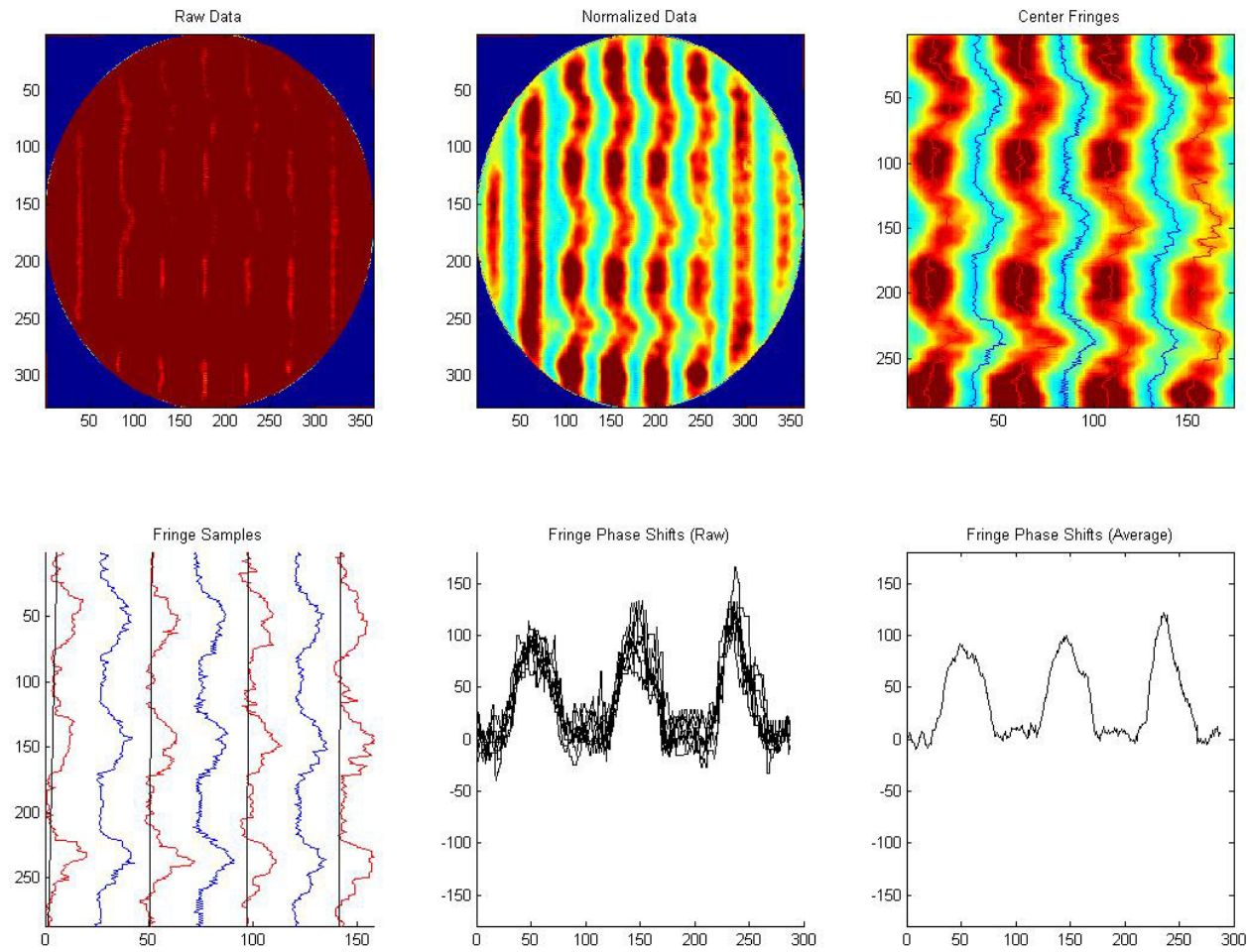


Figure 5.4: Averaged Phase Response Results for First SMIR

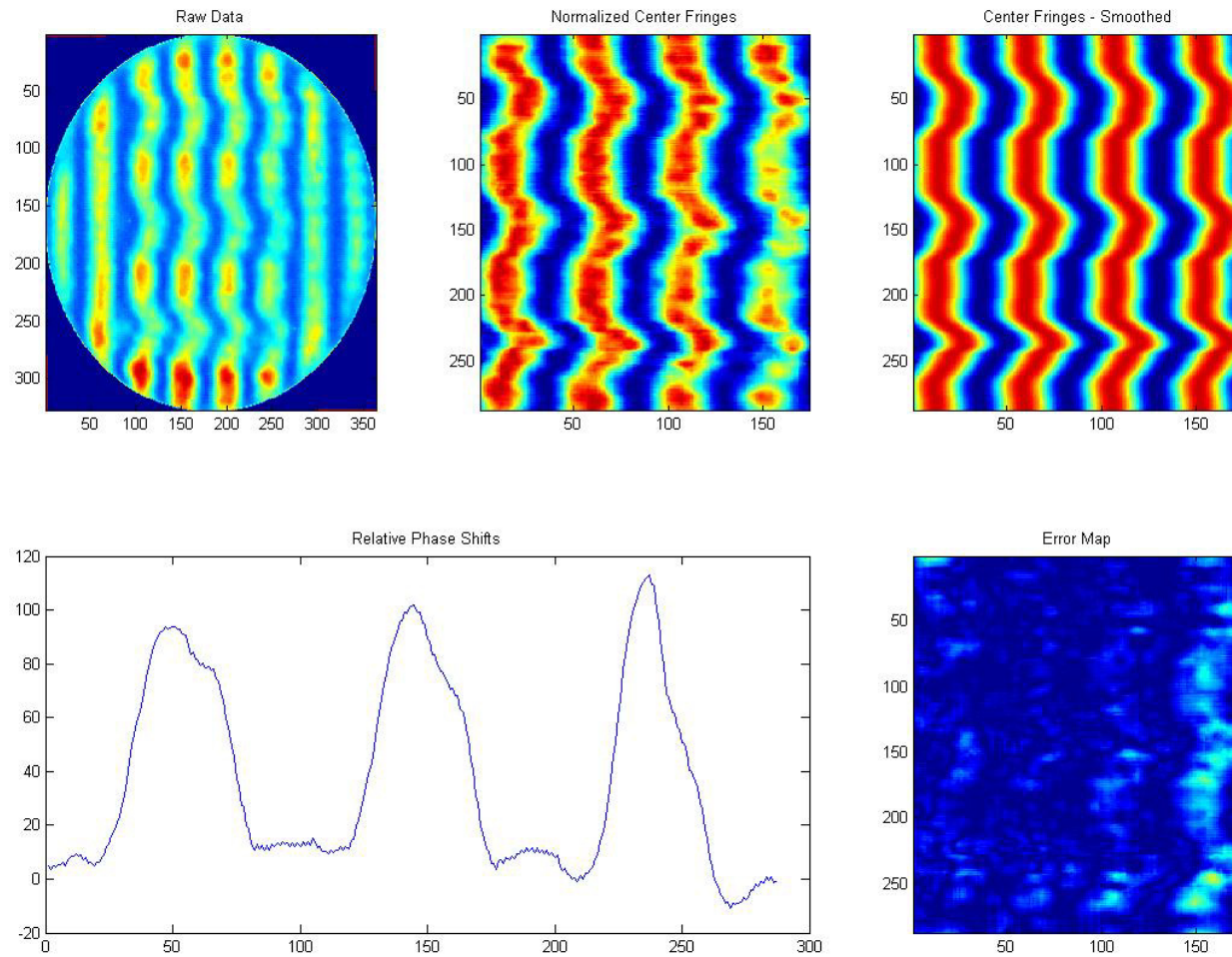


Figure 5.5: Smoothed Phase Response Results for First SMIR

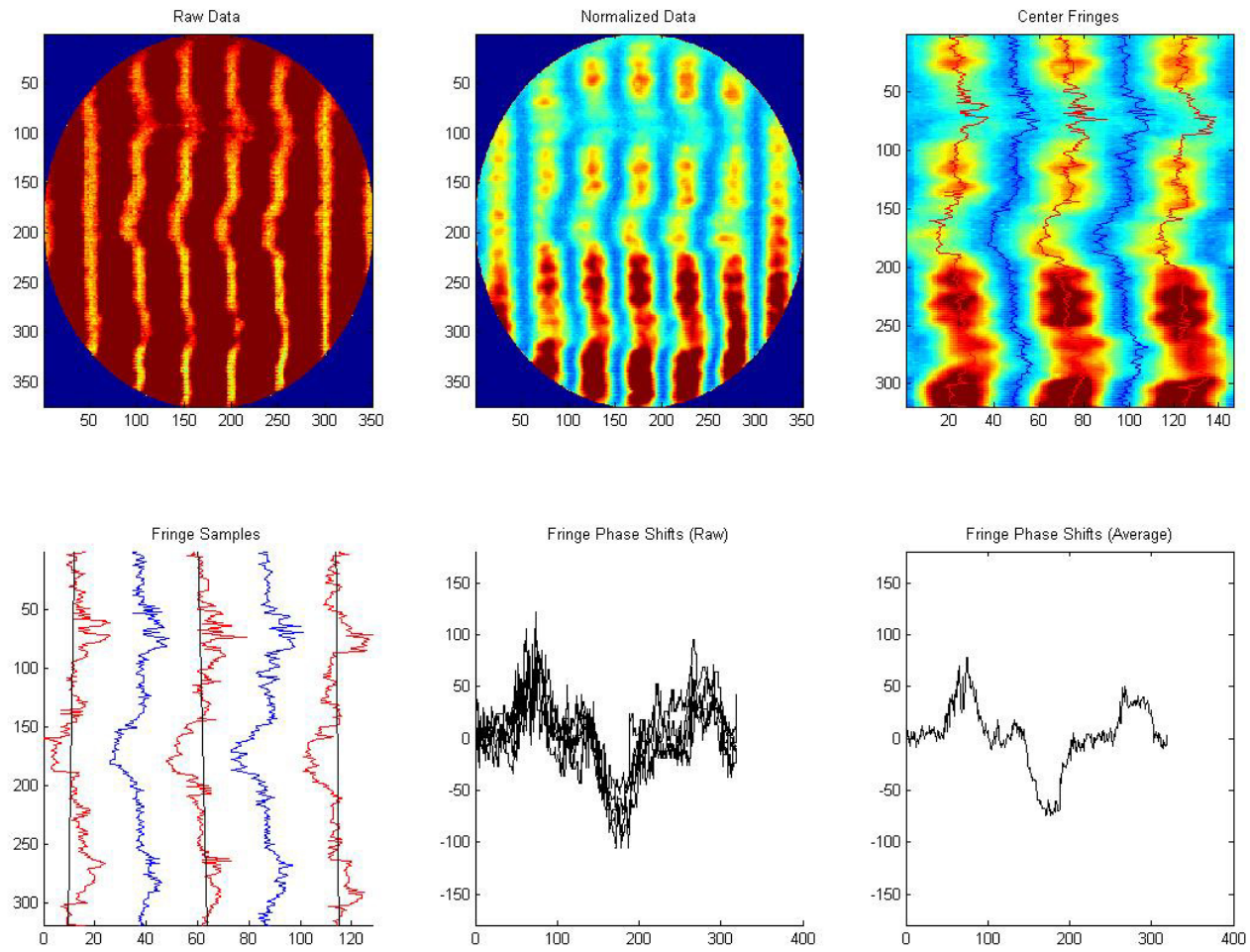


Figure 5.6: Averaged Phase Response Results for Second SMIR



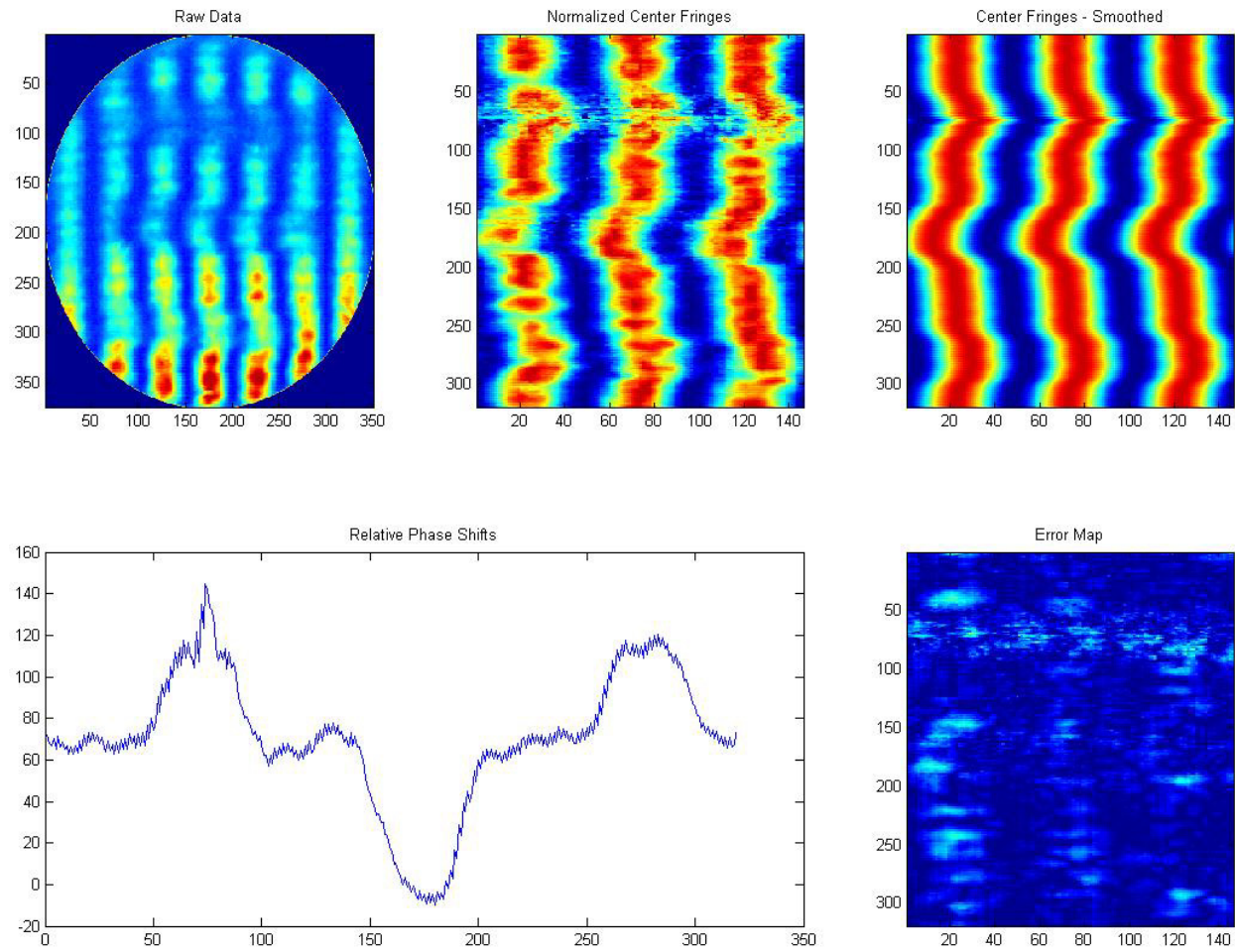


Figure 5.7: Smoothed Phase Response Results for Second SMIR

To determine the actual phase shift introduced by the reflectarray stripes, a correction factor was introduced to account for the double pass offset due to the height difference between the reference groundplane and the reflectarray patches. Using Eq. 5-1, the double pass phase shift for a 450 nm stand-off layer with a permittivity of 2.0 was calculated to be 43.4 degrees. By subtracting the phase offset from the values generated by the MATLAB function analysis, the phase shift introduced by the reflectarray was calculated and is summarized for the two proof of concept devices in Table 5.1.

**Table 5.1: Measured Relative Phase Shift vs. Reflectarray Patch Size**

<b>Patch Size</b>	<b>Relative Phase Shift Upon Reflection</b>
2.74 $\mu\text{m}$	174.4 $^{\circ}$
2.84 $\mu\text{m}$	172.4 $^{\circ}$
2.98 $\mu\text{m}$	136.4 $^{\circ}$
3.14 $\mu\text{m}$	124.1 $^{\circ}$
3.24 $\mu\text{m}$	110.3 $^{\circ}$
3.34 $\mu\text{m}$	-56.2 $^{\circ}$



## CHAPTER 6: CONCLUSIONS

### 6.1 Summary of Results

As illustrated from both modeled and measured results, the two SMIR proof of concept devices demonstrated that reflectarray behavior is feasible at IR with unique phase shifts measured across the reflectarray stripes. It is also possible to conclude from the results that fringe shifting occurs entirely due the difference in size of the patches and not due to a physical height difference used in conventional polished optics or reflector antennas. With the exception of the 3.34  $\mu\text{m}$  patch size, which is probably an extraneous sample point due to impurities introduced during fabrication, the measured phase response of each of the stripes correspond reasonably well with the Periodic MoM model (Figure 6.1) with a maximum demonstrate phase shift of approximately 70 degrees. Although highly promising, further testing will be necessary before a practical reflectarray can be designed and fabricated. In addition, adaptation and modification of both reflectarray models will be necessary if accurate prediction of reflectarray behavior is desired, especially if designs that are more complicated are developed.

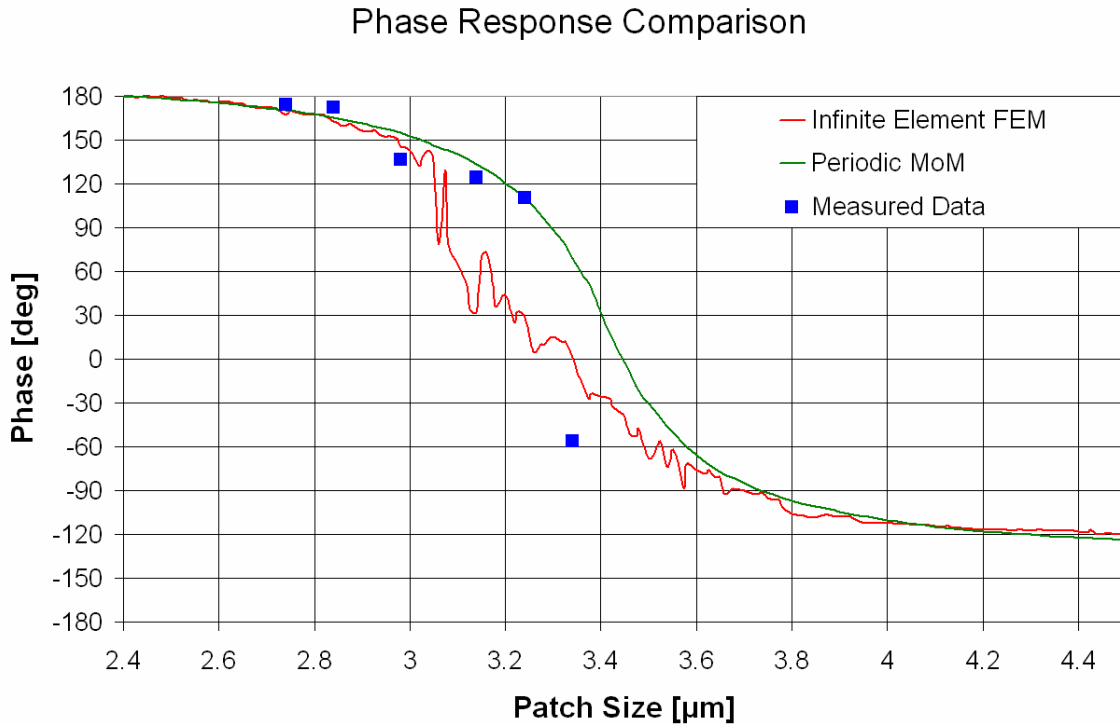


*Figure 6.1: Comparison of Measured and Modeled Results*

An interesting, albeit unintended, result of the thesis is the successful development and testing of an IR Electromagnetic (sometimes called a Photonic) Bandgap (EBG) structure fabricated using lithography techniques. In principle, EBG devices are very similar to reflectarrays in that they are a periodic arrangement of resonant structures that exhibit an arbitrary reflected phase response that varies over wavelength. Unlike reflectarrays, EBGs are usually designed to have a single, uniform phase response across the entire surface of the device at a single frequency for the purpose of creating high permittivity substrates, perfect magnetic conductors (PMC), or compressed groundplanes, analogous to the single patch size reflectarray stripes measured. EBG devices are a relatively new technology that has been grouped under the nebulous definition of “metamaterials” and debate continues in the engineering community if the devices should be regarded as true bandgap structures. EBG devices

have already been developed lithographically at RF and millimeter wave wavelengths [6.1 – 6.3]; however, most IR EBGs rely on the use of crystal photonic band structures [6.4 – 6.5]. As such, an IR EBG fabricated using lithography has the potential to bring further flexibility and lower costs to IR EBG design by relaxing the material requirements inherent in crystal designs.

## **6.2 Future Work**

### **6.2.1 Planar Tilt and Focusing Elements**

The next logical step for the development of the SMIR is to increase the number of sampled patch sizes. The easiest way to accomplish this would be to form a single stripe of reflectarray elements and gradually change the size of the patches in the reflectarray down the face of the wafer to create a tilt reflectarray. When testing in an interferometer, it should be possible to image the entire phase curve across the array, not just at a series of distinct points like in the thesis. Additionally, this reflectarray layout will allow preliminary investigation on the impact of phase response when placing different sized elements next to one another.

Of all the potential uses for an SMIR, a planar focusing IR reflectarray would be the most desirable and one of the easiest to develop after the testing of the tilt reflectarray. Optical imaging systems, such as cassegrains, could directly benefit from the reduction in size, weight, and cost through the replacement of traditional polished reflectors with SMIRs. Development of an SMIR planar focusing element would follow the same procedure as the one used at RF and millimeter-wave. By utilizing measured or

modeled reflection data relative to patch size, it is straight forward to calculate the array layout necessary to create the desired phase shift to correct for the change in path length between an arbitrary element and the center element to the focus point using ray tracing. This is further aided by the fact of the planar focusing elements will be either spherically or parabolically symmetric. Additionally, reflectarrays will follow the same design procedures as traditional reflector antennas in terms of gain and grating.

One issue of merit involves the fact that calculated lengths may not be feasible due to fabrication tolerances, especially when considering the size of the reflectarray relative to wavelength at IR. To overcome this restriction, it may be necessary to use the same patch size to cover a specific phase range. The detrimental effect of this approximation must be characterized in terms of aberration behavior; however, if it is determined not have a significant impact on performance, further element repetition will be investigated as a technique to reduce design complexity.

### **6.2.2 EBGs and Antenna Miniaturization**

One of the unique abilities of EBG surfaces is the ability to exhibit in-phase reflection for groundplane compression. To achieve maximum forward radiation efficiency, most planar antennas will utilize a groundplane with a quarter-wave stand-off layer. The 180 degrees of phase shift from the double pass stand-off layer, along with a 180 degree phase shift introduced upon reflection of the PEC groundplane allows for back radiated fields from the antenna to arrive back in phase at the antenna and add collectively with the forward radiated fields for optimal power delivery. If the stand-off layer is lossy, as often the case at IR frequencies, the quarter wave stand-off layer is less

effective as back radiated fields will be highly attenuated. To overcome this limitation, an EBG surface could be fabricated with a zero degree phase shift and the antenna could be fabricated directly on the surface, removing any losses introduced by the stand-off layer. In addition, as discussed in the design section of the thesis, most patch reflectarrays use stand-off layers significantly less than a quarter wave which would be beneficial in flexible substrate designs where thicker stand-off layers would break or crack upon flexing.

### **6.2.3 Bandwidth Improvement**

The greatest limitation of a variable-patch reflectarray is the device's limited bandwidth. Conventional reflective optical components, such as mirrors, traditionally have large operating bandwidths dependent entirely on material properties and physical dimensions. As demonstrated through transmission line equivalent circuit analysis, reflectarray bandwidth is defined by the frequency band that generates patch resonance, which is directly related to the dielectric height and patch sizes relative to wavelength. Three possible approaches are possible to achieve bandwidth improvement in SMIRs: developing multi-band layouts, controlling electromagnetic properties of fabrication materials, and stacking reflectarray layers.

The first approach to improving bandwidth would involve variation of the patch layout to create multi-band reflectarrays. In this approach, dielectric height is fixed, however, patches are arranged to demonstrate multiple resonant frequencies. Design of multi-band reflectarrays are inherently difficult, due to the non-uniform element spacing at higher frequencies and are difficult to design to achieve more than two bands of

resonance. Additionally, multi-band reflectarrays are not capable of continuous behavior between the two operating bands – limiting broadband operation.

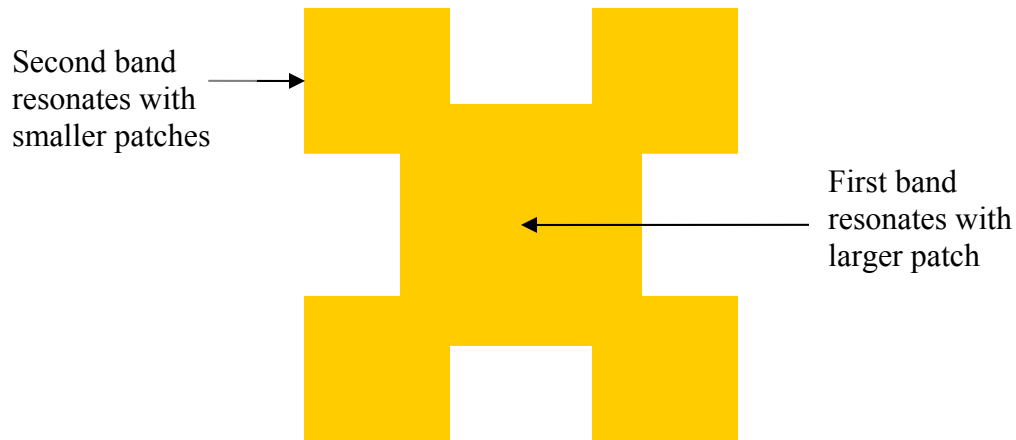


*Figure 6.2: Example Multi-band Reflectarray Layout*

Another approach to improving reflectarray bandwidth requires varying the material properties of the materials making up the structure. The easiest means to achieve bandwidth improvement by material variation is through controlled alteration of the substrate's permittivity. By replacing the SMIR substrate with a piezoelectric or doped material and biasing the device, it is possible to tune the substrate permittivity using the bias voltage to shift reflectarray resonance to a specific frequency band. Unlike the multi-band layout, however, the reflectarray will still be limited to a single, narrow band of operation at a fixed applied voltage. A related approach would be to directly exploit the natural dispersive properties of most materials at IR. Zirconium Dioxide, for example, exhibits a nearly linear transition in permittivity from around 7 to 12  $\mu\text{m}$  (Figure: 6.3). By tailoring the reflectarray design to utilize this linear shift, it might be possible to expand the bandwidth of the reflectarray without the need of an exotic substrate.

## ZrO<sub>2</sub> - Measured Dielectric Properties

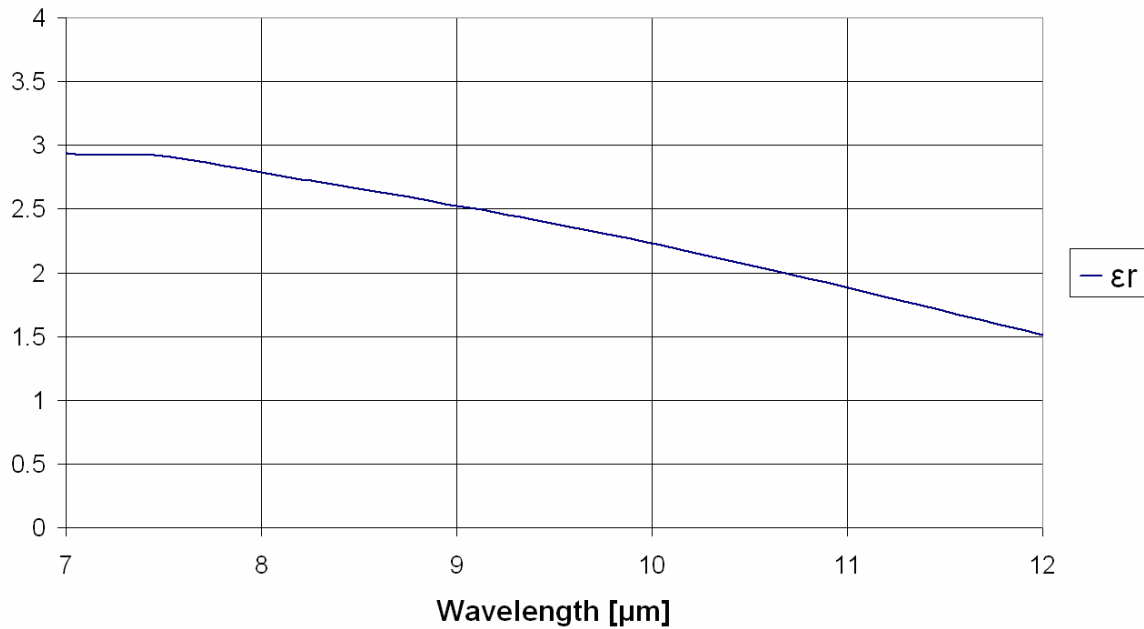
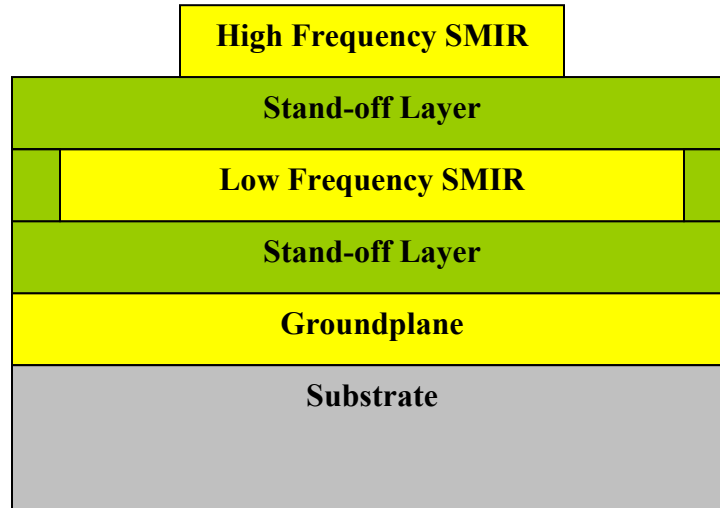


Figure 6.3: Measured Permittivity of ZrO<sub>2</sub> Exhibiting Linear Transition

The final approach to improving reflectarray bandwidth is through element stacking. Current research at microwave and millimeter frequencies has demonstrated that stacking of reflectarray layers on top of one another will result in multiple bands of operation and, if desired, these bands can be continuous [6.6 – 6.8]. The principle of reflectarray stacking can be approached simply by applying the reflectarray transmission line approximation. Begin by considering a two layer reflectarray. If the reflectarray layers are stacked in a way that the top layer resonates at higher frequency than the lower layer, the lower layer will behave as a lossy groundplane for the top layer and form a functioning reflectarray. At lower frequencies, the top layer will be relatively transparent and only the bottom layer and the groundplane will introduce reflectarray behavior. The main limitation of stacked reflectarrays is the increase in material losses due to the

introduction of multiple metal layers and the increased complexity in modeling reflectarrays inherent with more than two layers.



*Figure 6.4: Stackup for a Multi-Layer Reflectarray*

### 6.2.4 Aberration Correction

Two issues must be considered when discussing aberration correction and SMIRs: correction of aberrations introduced by reflectarrays in an optical system and using reflectarrays to correct for aberrations in an optical system. For the first case, very little research has been carried out to analyze reflectarray aberration behavior largely because, prior to this thesis, all reflectarray research has been at lower frequencies, where system aberrations are less significant for proper operation. Never the less, characterization of SMIR aberrations can be directly analyzed using interferometry. The SMIR should demonstrate the same monochromatic aberrations as an ideal reflector, but, due to material dispersion and patch size mismatches, significant chromatic aberrations will be present unless bandwidth is improved.



The second aberration correction case, static correction of system aberration using SMIRs, is especially interesting. For example, if the spherical aberration of an optical system was known, a reflectarray layout can be designed for to introduce a phase shift, or defocus, to offset the spherical aberration. Similarly, tilt could be corrected by introducing a linear phase shift across the reflectarray surface. The other third and higher order aberrations (coma, astigmatism, etc.) would be more difficult to correct for using a reflectarray only, but, with proper analysis, reflectarrays may still play a significant role, especially considering their design flexibility.

### **6.2.5 Further Cost Reduction**

In its initial form, the designed reflectarray would still be expensive to fabricate and deploy. Several cost reduction techniques should be considered and are outlined in Table 6.1.

**Table 6.1: Further Reflectarray Cost Reduction Techniques**

<b>Issue</b>	<b>Possible Solution</b>
High Cost of Metals	Several metals can be deposited in place of gold, including silver and aluminum. Although hampered by a native oxide layer, Aluminum would exhibit better performance than gold due to its higher reflectivity at MWIR and LWIR.
High Cost of E-beam Lithography	From about 8 – 12 $\mu\text{m}$ , the necessary reflectarray patch sizes should be large enough to utilize optical lithography or nano-imprint technology. Both of these approaches are cheaper than e-beam lithography and are better suited for mass production.
High Cost of Optical Flat	The main purpose of the optical flat is to insure no fringe shifting is introduced by the substrate. As SMIR technology matures, studies will be carried out to characterize what tolerances restrict reflectarray operation and cheaper substrates can be employed.

## LIST OF REFERENCES

- [1.1] B. Van Veen and K. Buckley, "Beamforming: A versatile approach to spatial filtering," IEEE ASSP Magazine, vol. 5, no. 2, Apr. 1988, pp. 4-24.
- [1.2] E Bedrosian, "The curved passive reflector," IEEE Transactions on Antennas and Propagation, vol. 3, no. 4, Oct 1955, pp. 168-173.
- [1.3] T. Pratt, C. Bostian, and J. Allnut, "Satellite Communications," Wiley, 2003.
- [1.4] F. Brickell, L. Marder, and B. Westcott, "The geometrical optics design of reflectors, using complex coordinates," J. Phys. A.: Math. Gen., vol. 10, no. 2, 1977, pp. 245-260.
- [1.5] R. Fante, and R. Taylor, "Near-field distribution of a paraboloidal reflector," IEEE Transactions on Antennas and Propagation, vol. 25, no. 4, Jul 1977, pp. 589 – 590.
- [1.6] J. Bergmann, F. Hasselmann, F. Teixeira, and C. Rego, "A comparison between techniques for global surface interpolation in shaped reflector analysis," IEEE Transactions on Antennas and Propagation, vol. 42, no. 1, Jan. 1994, pp. 47 – 53.
- [1.7] W. Welford, "Aberations of Optical Systems," Adam Hilger, 1986.
- [1.8] H. Luh, "A puzzle in reflector shaping", 2002 IEEE Antennas and Propagation Society International Symposium, vol. 4, 16-21 June 2002, pp. 120 – 123.
- [1.9] M. Terada, and W. L. Stutzman, "Computer-aided design of reflector antennas," Microwave Journal, Aug. 1995, pp. 64–73.
- [1.10] C. Pell, "Phased-array radars," IEE Review, vol. 34, no. 9, 6 Oct. 1988, pp. 363 – 367.

- [1.11] C. Balanis, "Antenna Theory: Analysis and Design," Wiley-Interscience, ed. 3, 2005.
- [1.12] H. Schippers, G. Spalluto, and G. Vos, "Radiation analysis of conformal phased array antennas on distorted structures", Twelfth International Conference on Antennas and Propagation, vol. 1, 31 March-3 April 2003, pp. 160 – 163.
- [1.13] K. Shum, Q. Xue, C. Chan, K. Luk, "Investigation of microstrip reflectarray using a photonic bandgap structure," Microwave and Optical Technology Letters, vol. 18, no. 2, 2001, pp. 114-116.
- [1.14] J. Huang, "Capabilities of printed reflectarray antennas," IEEE International Symposium on Phased Array Systems and Technology, 15-18 Oct. 1996, pp. 131 – 134.
- [1.15] D. Berry, R. Malech, and W. Kennedy, "The reflectarray antenna," IEEE Transactions on Antennas and Propagation, vol. 11, no. 6, Nov 1963, pp. 645 – 651.
- [1.16] J. Montgomery, "Scattering by an infinite periodic array of microstrip elements," IEEE Transactions on Antennas and Propagation, vol. 26, no. 6, Nov 1978, pp. 850 – 854.
- [1.17] N. Misran, R. Cahill, and V. Fusco, "RCS reduction technique for reflectarray antennas," Electronics Letters, vol. 39, no. 23, 13 Nov. 2003, pp. 1630 – 1631.
- [1.18] D. Pozar, and T. Metzler, "Analysis of a reflectarray antenna using microstrip patches of variable size", Electronics Letters, vol. 29, no. 8, 15 April 1993 pp. 657 – 658.

- [1.19] A. Zaman, and R. Lee, "A spherical to plane wave transformation using a reflectarray," IEEE Antennas and Propagation Society International Symposium, vol. 2, 13-18 July 1997, pp. 1284 – 1287.
- [1.20] A. Kelkar, "FLAPS conformal phased reflecting surfaces," Proceedings of the 1991 IEEE National Radar conference, 12-13 March 1991, pp. 58-62
- [1.21] D. Gonzalez, G. Pollon, and J. Walker, "Microwave phasing structures for electromagnetically emulating reflective surfaces and focusing elements of selected geometry," US Patent 4 905 014, Malibu Research Associates, February 1990.
- [1.22] From ILC Dover corporate website:  
[http://www.ilcdover.com/products/aerospace\\_defense/inflatableantenna.htm](http://www.ilcdover.com/products/aerospace_defense/inflatableantenna.htm)
- [1.23] From TRILabs corporate website:  
<http://www.trilabs.ca/trilabs/technology/technologybulletins/reconfigurableantenna.html>
- [2.1] F. Tsai, and M. Bialkowski, "Designing a 161-element Ku-band microstrip reflectarray of variable size patches using an equivalent unit cell waveguide approach," IEEE Transactions on Antennas and Propagation, Volume 51, Issue 10, Part 2, Oct. 2003, pp. 2953 – 2962.
- [2.2] D. Chang, and M. Huang, "Multiple-polarization microstrip reflectarray antenna with high efficiency and low cross-polarization" IEEE Transactions on Antennas and Propagation, vol. 43, no. 8, Aug. 1995, pp. 829 – 834.

- [2.3] F. Venneri, G. Angiulli, and G. Di Massa, "Design of microstrip reflect array using data from isolated patch analysis," *Microwave and Optical Technology Letters*, vol. 32, no. 6, 2002, pp. 411-414.
- [2.4] D. Pozar, and S. Targonski, "A microstrip reflectarray using crossed dipoles", *IEEE Antennas and Propagation Society International Symposium*, vol. 2, 21-26 June 1998, pp. 1008 – 1011.
- [2.5] Z. Wu, W. Zhang, Z. Liu, and W. Shen, "Circularly polarised reflectarray with linearly polarised feed" *Electronics Letters*, vol. 41, no. 7, 31 March 2005, pp. 387 – 388.
- [2.6] D. Pozar, "Bandwidth of reflectarrays," *Electronics Letters*, vol. 39, no. 21, 16 Oct. 2003, pp. 1490 – 1491.
- [2.7] D. Pozar, "Microwave Engineering," Wiley, ed. 3, 2005.
- [2.8] D. Pozar, S. Targonski, and H. Syrigos, "Design of Millimeter Wave Microstrip Reflectarrays," *IEEE Transactions on Antennas and Propagation*, vol. 45, no.2, February 1997, pp. 287 – 296.
- [2.9] Ansoft HFSS reference manual, Rel. 10, Ansoft Corporation, 2005.
- [2.10] Ansoft Designer reference manual, Rel. 2.1, Ansoft Corporation, 2004.
- [2.11] N. Lenin, and P. Rao, "Evaluation of the reflected phase of a patch using waveguide simulator for reflectarray design," *Microwave and Optical Technology Letters*, vol. 45, no. 6, 2005, pp. 528 – 531.
- [2.12] R. Jedlicka, M. Poe, and K. Carver, "Measured mutual coupling between microstrip antennas," *IEE Transactions on Antennas and Propagation*, vol. 29, no.1, January 1981, pp. 147 – 149.

- [3.1] J. Ginn, B. Lail, D. Shelton, J. Tharp, W. Folks, and G. Boreman, "Modeling infrared frequency selective surfaces with frequency dependent materials," The 22nd International Review of Progress in Applied Computational Electromagnetics, March 12 - 16, 2006, invited paper.
- [5.1] Image taken from:  
[http://microgravity.grc.nasa.gov/MSD/GRC\\_MSD\\_Graphics/FluidPhysics/78457TwymanGreenInterferome.pdf](http://microgravity.grc.nasa.gov/MSD/GRC_MSD_Graphics/FluidPhysics/78457TwymanGreenInterferome.pdf)
- [6.1] J. Shumpert,, W. Chappell, and L. Katehi, "Parallel-plate mode reduction in conductor-backed slots using electromagnetic bandgap substrates," IEEE Transactions on Microwave Theory and Techniques, vol. 47, no. 11, Nov. 1999, pp. 2099 – 2104.
- [6.2] C. Cheype, C. Serier, M. Thevenot, T. Monediere, A. Reineix, and B. Jecko, "An electromagnetic bandgap resonator antenna," IEEE Transactions on Antennas and Propagation, vol. 50, no. 9, Sept. 2002, pp. 1285 – 1290.
- [6.3] Fan Yang, and Y. Rahmat-Samii, "Reflection phase characterizations of the EBG ground plane for low profile wire antenna applications," IEEE Transactions on Antennas and Propagation, vol. 51, no, 10, Oct. 2003, pp. 2691 – 2703.
- [6.4] S. Rowson, A. Chelnokov, and J. Lourtioz, "Two-dimensional photonic crystals in macroporous silicon: from mid-infrared (10  $\mu\text{m}$ ) to telecommunication wavelengths (1.3-1.5  $\mu\text{m}$ )" Journal of Lightwave Technology, vol. 17, no. 11, Nov. 1999, pp. 1989 – 1995.

- [6.5] Younan Xia, B. Gates, and Sang Hyun Park, "Fabrication of three-dimensional photonic crystals for use in the spectral region from ultraviolet to near-infrared," *Journal of Lightwave Technology*, vol. 17, no. 11, Nov. 1999, pp. 1956 – 1962.
- [6.6] J. Encinar, "Design of two-layer printed reflectarrays using patches of variable size," *IEEE Transactions on Antennas and Propagation*, vol. 49, no. 10, Oct. 2001, pp. 1403 – 1410.
- [6.7] D. Wu, R. Hall, J. Huang, "Dual-frequency microstrip reflectarray," *Antennas and Propagation Society International Symposium*, vol. 4, 18-23 June 1995, pp. 2128 – 2131
- [6.8] J. Zornoza, and M. Bialkowski, "Design of a shaped beam multi-layer microstrip reflectarray with Australia and New Zealand coverage pattern," *IEEE International Symposium on Phased Array Systems and Technology*, 14-17 Oct. 2003, pp. 488 – 493.